Missouri S&T Library and Learning Resources

Scholars' Mine

Doctoral Dissertations

Student Theses and Dissertations

Summer 2015

Resistance switching of electrodeposited cuprous oxide

Sanaz Yazdanparast

Follow this and additional works at: https://scholarsmine.mst.edu/doctoral_dissertations

Part of the Materials Science and Engineering Commons

Department: Materials Science and Engineering

Recommended Citation
Yazdanparast, Sanaz, "Resistance switching of electrodeposited cuprous oxide" (2015). *Doctoral Dissertations*. 2424.
https://scholarsmine.mst.edu/doctoral_dissertations/2424

This thesis is brought to you by Scholars' Mine, a service of the Missouri S&T Library and Learning Resources. This work is protected by U. S. Copyright Law. Unauthorized use including reproduction for redistribution requires the permission of the copyright holder. For more information, please contact scholarsmine@mst.edu.

RESISTANCE SWITCHING OF ELECTRODEPOSITED CUPROUS OXIDE

by

SANAZ YAZDANPARAST

A DISSERTATION

Presented to the Faculty of the Graduate School of the

MISSOURI UNIVERSITY OF SCIENCE AND TECHNOLOGY

In Partial Fulfillment of the Requirements for the Degree

DOCTOR OF PHILOSOPHY

in

MATERIALS SCIENCE AND ENGINEERING

2015

Approved by

Jay A. Switzer, Advisor
Wayne Huebner
Scott Miller
Michael Moats
Maceij Zawodniok

© 2015

Sanaz Yazdanparast

All Rights Reserved

PUBLICATION DISSERTATION OPTION

This dissertation has been prepared based on three manuscripts for publication. The first paper “COPPER NANOFILAMENT FORMATION DURING UNIPOLAR RESISTANCE SWITCHING OF ELECTRODEPOSITED CUPROUS OXIDE” has been submitted to *Chemistry of Materials*. The second paper “THE EFFECTIVE PARAMETERS ON RESISTANCE SWITCHING OF ELECTRODEPOSITED CUPROUS OXIDE THIN FILMS” has been prepared for submission to *Materials and Design*. And the third paper” RESISTANCE SWITCHING OF ELECTRODEPOSITED Cu_2O NANOWIRES” has been prepared for submission to *Applied Physics Letters*.

The SECTION portion of this dissertation has three parts. The first part presents the current state of research on resistance switching which includes: 1) classification of resistance switching behavior, 2) performance parameters of resistance switching random access memory (RRAM), 3) resistance switching mechanisms, 4) a literature review on resistance switching of metallic oxides, and 5) processing methods and properties of cuprous oxide. The second part includes the objectives and potential impacts. The last part is the overall conclusion of this work as well as some suggestions for future research in the area of resistance switching of cuprous oxide.

ABSTRACT

In this work, the resistance switching behavior of electrodeposited cuprous oxide (Cu_2O) thin films in Au/Cu_2O/top electrode (Pt, Au-Pd, Al) cells was studied. After an initial FORMING process, the fabricated cells show reversible switching between a low resistance state (16.6 Ω) and a high resistance state (0.4×10^6 Ω). Changing the resistance states in cuprous oxide films depends on the magnitude of the applied voltage which corresponds to unipolar resistance switching behavior of this material. The endurance and retention tests indicate a potential application of the fabricated cells for nonvolatile resistance switching random access memory (RRAM). The results suggest formation and rupture of one or several nanoscale copper filaments as the resistance switching mechanism in the cuprous oxide films. At high electric voltage in the as-deposited state of Au/Cu_2O/Au-Pd cell structure, the conduction behavior follows Poole-Frenkel emission. Various parameters, such as the compliance current, the cuprous oxide microstructure, the cuprous oxide thickness, top electrode area, and top electrode material, affect the resistance switching characteristics. The required FORMING voltage is higher for Au/Cu_2O/Al cell compared with the Au/Cu_2O/Pt which is related to the Schottky behavior of Al contact with Cu_2O. Cu_2O nanowires in Au-Pt/ Cu_2O/Au-Pt cell also show resistance switching behavior, indicating scalable potential of this cell for usage as RRAM. After an initial FORMING process under an electric field of 3×10^6 V/m, the Cu_2O nanowire is switched to the LRS. During the FORMING process physical damages are observed in the cell, which may be caused by Joule heating and gas evolution.

ACKNOWLEDGMENTS

I would like to thank my Ph.D. advisor, Prof. Jay A. Switzer for his guidance and support during my Ph.D. study. I would also like to thank Prof. Wayne Huebner, Prof. Scott Miller, Prof. Michael Moats, and Prof. Maceij Zawodniok for serving as my dissertation committee members.

I would like to thank the members of Prof. Switzer's research group, especially Dr. Jakub Koza, Allen Liu, and Naveen Mahenderkar for their help in conducting some of my experiments. I would also like to thank Dr. Jessica Terbush, Dr. Clarissa Wisner, and Dr. Eric Bohannan for their help in characterization experiments. In addition, I would like to thank the staff in the Department of Materials Science and Engineering and Materials Research Center.

A special thanks to my parents for their love and support throughout my life. Last but not least, my deepest gratitude goes to my husband, Prof. Mohsen Asle Zaeem who supported me through my studies and for his every day encouragement which has been a source of inspiration for me throughout my life.

TABLE OF CONTENTS

Page

ABSTRACT iv

ACKNOWLEDGMENTS v

LIST OF ILLUSTRATIONS ix

LIST OF TABLES xii

NOMENCLATURE xii

SECTION

1. CURRENT STATE OF RESEARCH ON RESISTANCE SWITCHING……..…1

1.1 OVERVIEW 1

1.2 CLASSIFICATION OF RESISTANCE SWITCHING BEHAVIOR.........2

1.3 PERFORMANCE PARAMETERS OF RRAM..4

1.3.1 Endurance 4

1.3.2 Retention or Stability 4

1.3.3 Operating Voltage..4

1.4 RESISTANCE SWITCHING MECHANISMS 4

1.4.1 Conduction Mechanism in LRS...4

1.4.2 Conduction Mechanism in HRS 6

1.5 LITERATURE REVIEW ON RESISTANCE SWITCHING OF METALLIC OXIDES...8

1.5.1 Resistance Switching of Cu_2O and CuO..8

1.5.2 Resistance Switching of NiO 9

1.5.3 Resistance Switching of TiO_2 11

1.5.4 Resistance Switching of ZnO....................12

1.5.5 Resistance Switching of Other Oxides 13

1.6 PROCESSING METHODS AND PROPERTIES OF CUPROUS OXIDE 14

2. RESEARCH OBJECTIVES AND IMPACTS 15

PAPER

I. COPPER NANOFILAMENT FORMATION DURING UNIPOLAR RESISTANCE SWITCHING OF ELECTRODEPOSITED CUPROUS OXIDE 17

ABSTRACT....................18

INTRODUCTION 19

EXPERIMENTAL....................20

RESULTS AND DISCUSSION....................22

CUPROUS OXIDE THIN FILMS 22

DC AND AC CHARACTERISTICS OF AS-DEPOSITED CUPROUS OXIDE THIN FILMS 24

FORMATION OF COPPER NANOFILAMENT IN RESISTANCE SWITCHING OF Cu_2O....................31

STUDYING THE RESISTANCE SWITCHING MECHANISM OF Cu2O 39

CONCLUSIONS....................43

ACKNOWLEDGMENTS 44

II. THE EFFECTIVE PARAMETERS ON RESISTANCE SWITCHING OF ELECTRODEPOSITED CUPROUS OXIDE THIN FILMS....................45

ABSTRACT....................46

INTRODUCTION 47

EXPERIMENTAL PROCEDURE 48

RESULTS 49

CONCLUSIONS..62

ACKNOWLEDGMENTS 63

III. RESISTANCE SWITCHING OF ELECTRODEPOSITED Cu_2O NANOWIRES …………………… 64

ABSTRACT..65

INTRODUCTION 66

EXPERIMENTAL PROCEDURE 67

RESULTS 68

CONCLUSIONS...70

ACKNOWLEDGMENTS 71

SECTION

3. CONCLUSIONS AND SUGGESTIONS FOR FUTURE WORKS 72

APPENDICES

A EFFECT OF CUPROUS OXIDE THICKNESS ON FORMING VOLTAGE …………………… 74

B EFFECT OF TOP ELECTRODE MATERIAL ON FORMING VOLTAGE …………………… 76

BIBLIOGRAPHY 80

VITA…………………………………………………………………………..91

LIST OF ILLUSTRATIONS

SECTION Page

Figure 1.1 Current-voltage (I-V) curves of unipolar and bipolar resistance switching. 3

PAPER I

Figure 1. XRD pattern of electrodeposited cuprous oxide thin film (5 μm in thickness) on gold coated glass substrate 23

Figure 2. X-ray pole figure of [111]-oriented cuprous oxide on Au-coated glass 23

Figure 3. Top-view SEM image of cuprous oxide grains in a 5 μm thick film 24

Figure 4. Schematic of resistance switching cell 25

Figure 5. Current-voltage characteristic of Au/Cu_2O (5 μm in thickness)/Au-Pd cell during FORMING, RESET and SET steps 26

Figure 6. Endurance of the Au/Cu_2O (5 μm thick)/Au-Pd cell 27

Figure 7. Retention characteristics of Au/Cu_2O(5 μm in thickness)/Au-Pd cell in each state of LRS and HRS 28

Figure 8. Impedance spectra of three different states of Au/Cu_2O (5 μm thick)/Au-Pd cell 30

Figure 9. Resistance vs. temperature plots of the Au/Cu_2O (2 μm thick)/In cell in as-deposited state and HRS b) The Arrhenius plots of the as-deposited state and HRS 32

Figure 10. Resistance vs. temperature plot of the Au/Cu_2O (2 μm thick))/In cell in LRS with its linear fit 34

Figure 11. Diameter of the filament vs. compliance current in Au/Cu_2O(5 μm thick)/Au-Pd cell 35

Figure 12. Corresponding RESET plots of Cu filaments with diameter of a) 73.7 nm which was formed at compliance current of 18 mA, and b) 115 nm which was formed at compliance current of 50 mA.. 36

Figure 13. The effect of compliance current on RESET current in Au/Cu_2O (5 μm in thickness)/Au-Pd cell. 38

Figure 14. The effect of compliance current on RESET voltage and current density in Au/Cu_2O (5 μm in thickness)/Au-Pd cell.. 39

Figure 15. Log I-Log V curve of FORMING process showing linear and non-linear behavior at low and high electric voltage, respectively. 41

Figure 16. Poole-Frenkel emission plot of as-deposited state at high electrical voltage (14.3-19.4 V).. 41

Figure 17. Current-voltage curve of Au/Cu_2O (5 µm thick)/Au-Pd cell during RESET process with calculated temperatures in each region of the plot before rupturing the nanofilament. 43

PAPER II

Figure 1. XRD results of electrodeposited cuprous oxide films at constant temperature of 50^0 C and different potentials.. 50

Figure 2. Cross section SEM images of electrodeposited films at -0.394 V and -0.283 V 51

Figure 3. Plan view SEM images of cuprous oxide grains electrodeposited at different potentials.... 52

Figure 4. XRD results of electrodeposited cuprous oxide films at constant cathodic current density of $1mA/cm^2$ and different temperatures.... 53

Figure 5. Cross-sectional SEM images of electrodeposited films at 25° C and 40° C..... 54

Figure 6. Plan view SEM images of cuprous oxide grains electrodeposited at different temperatures..... 55

Figure 7. The required FORMING voltage for the cuprous oxide films electrodeposited at different potentials..... 57

Figure 8. The required FORMING voltage for the cuprous oxide films electrodeposited at galvanostatic mode and different temperatures...... 58

Figure 9. SET and RESET voltages as a function of average grain size of cuprous oxide 59

Figure 10. HRS and LRS current levels vs. average grain size of cuprous oxide.. 60

Figure 11. FORMING voltage vs. top electrode area. 61

Figure 12. Current of LRS and HRS as a function of top electrode area.. 62

PAPER III

Figure 1. Schematic of growing Cu_2O nanowires.. 68

Figure 2. Scanning electron microscopy (SEM) images of a Cu_2O nanowire connected to Au pads using electron beam and deposition of Pt......................... 69

Figure 3. I-V curve of FORMING process showing switching the Cu_2O nanowire to the LRS... 69

Figure 4. SEM image of Pt/ Cu_2O nanowire/Pt cell after FORMING............................. 70

LIST OF TABLES

PAPER I Page

Table 1. Summary of equivalent circuit parameters obtained from impedance spectroscopy at three different states. 31

PAPER II

Table 1. The measured resistance from impedance spectroscopy for Au/Cu_2O/Au-Pd cell with three different top electrode areas.. 62

NOMENCLATURE

Symbol	Description
μ	Carrier mobility ($cm^2.V^{-1}.s^{-1}$)
ε_o	Permittivity of free space ($F.cm^{-1}$)
ε_i	Dynamic dielectric constant (dimensionless)
L	Thickness of the film (cm)
A	Cross sectional area of top electrodes (cm^2)
V	Electric voltage (V)
I	Current ($C.s^{-1}$)
q	Electron charge (C)
k_B	Boltzmann's constant ($J.K^{-1}$)
m^*	Effective electron mass in dielectric (Kg)
h	Planck's constant (J.s)
T	Temperature (K)
ϕ_B	Schottky barrier height (eV)
N_C	Density of states in the conduction band (cm^{-3})
ϕ_t	Trap energy barrier height (eV)
α	Resistance temperature coefficient (K^{-1})
d	Diameter of filament (nm)
R	Resistance (Ω)
ρ	Resistivity (Ω.cm)

SECTION

1. CURRENT STATE OF RESEARCH ON RESISTANCE SWITCHING

1.1 OVERVIEW

Due to the high demand of portable electronic devices such as smartphones and laptops in modern life, the development of high speed, high density, and low power semiconductor memories is necessary [1-3]. Semiconductor memories can be classified as volatile and nonvolatile memories [4]. Dynamic RAMs (DRAMs) and Static RAMs (SRAMs) are examples of volatile memories, and unlike nonvolatile memories they lose their storage data when the power is interrupted [4, 5]. The current nonvolatile FLASH memory which is based on charge storage has a scalability problem because as the size of the device is decreased it becomes increasingly difficult to retain charge. Among several types of non-volatile memories [4, 6], resistance switching random access memory (RRAM) has attracted recent attention because of its high scalability, easy fabrication, and multibit storage potential [5, 7-12]. A RRAM has a simple cell structure composed of an insulating or oxide material sandwiched between two metal electrodes [13]. There are different types of materials that show resistance switching behavior, e.g. perovskites such as $SrZrO_3$ [2, 14, 15], chalcogenides such as Ag_2S, Cu_2S [16, 17], and binary transition metal oxides such as TiO_2, NiO, CuO, and Cu_2O [18-20]. Among these materials, binary transition metal oxides are receiving increasing interest due to their simple composition, thermal stability, and compatibility with complementary metal–oxide-semiconductor (CMOS) technology [5, 21, 22].

RRAM is based on reversible switching of the insulating material between high and low resistance states [23-25]. Typically, a high electric voltage with a limited compliance current is necessary to initiate the reversible switching [26-30]. This initial step in resistance switching is called the FORMING process which switches the as-deposited state of the material to the low resistance state (LRS). The second step in resistance switching is the RESET process in which the material switches to the high resistance state (HRS) by applying a low voltage with no compliance current. The third step in resistance switching is called the SET process which is similar to the FORMING process except in the SET process a lower voltage is required to switch the material to the LRS [31, 32]. The purpose of using a compliance current in both the FORMING and SET process is to avoid permanent dielectric breakdown of oxide materials in resistance switching process [4, 11].

1.2 CLASSIFICATION OF RESISTANCE SWITCHING BEHAVIOR

Based on the current-voltage (I-V) characteristics, resistance switching can be classified as either unipolar and bipolar switching [3, 11, 33, 34]. In unipolar switching, the required voltages in SET and RESET steps are of the same polarity with different magnitude [6, 35] while in bipolar switching they are of opposite polarity [36, 37]. Figure 1.1 shows I-V curves of unipolar and bipolar switching. These different switching behaviors can be dependent on the involved materials in RRAM; including the intermediate layer and both top and bottom electrodes [32, 38, 39].

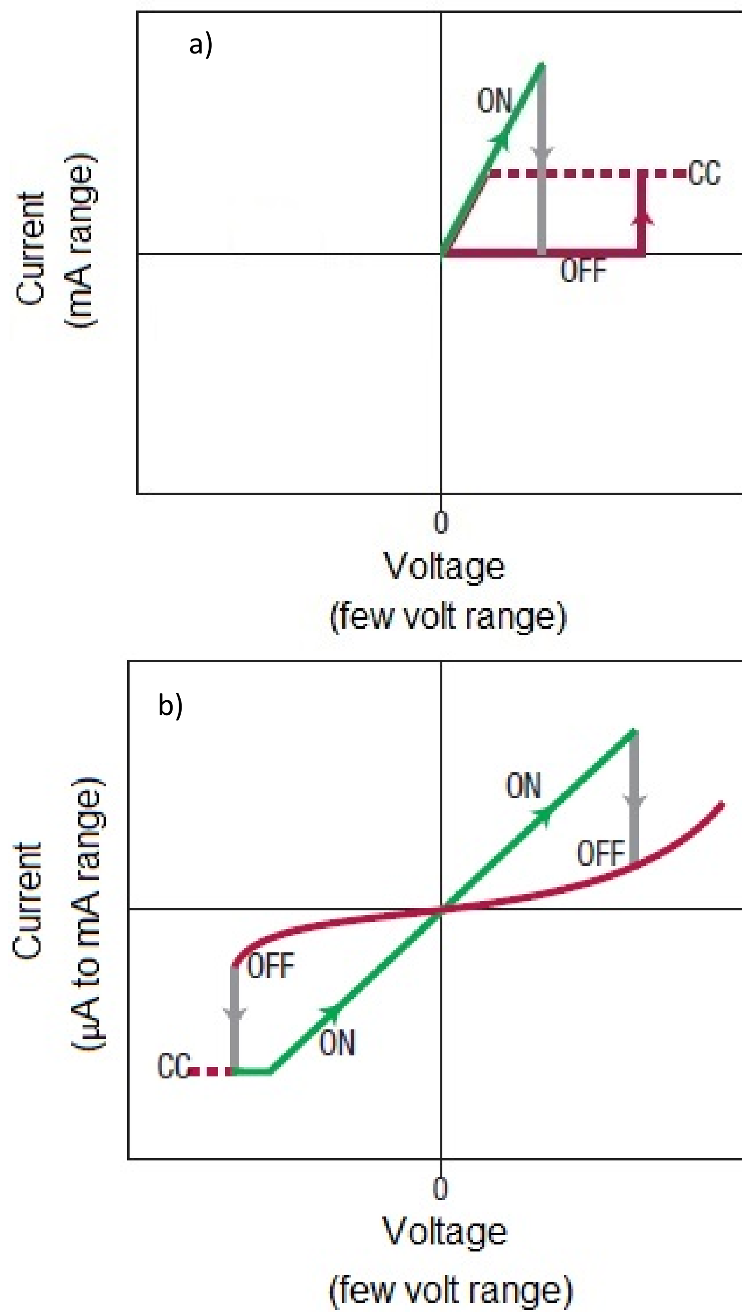

Figure 1.1 Current-voltage (I-V) curves of a) unipolar and b) bipolar resistance switching The ON and OFF states correspond to the LRS and HRS, respectively. CC is the compliance current. Reproduced from reference [40].

1.3 PERFORMANCE PARAMETERS OF RRAM

Since resistance switching has been proposed as a promising candidate for next generation nonvolatile memories, it is necessary to study the important performance parameters of RRAM such as endurance, retention or stability, and operating voltage.

1.3.1 Endurance. An RRAM device should have a large endurance ($\geq 10^6$ cycles). Endurance shows how many cycles a memory device can be switched between HRS and LRS before these two states are no longer distinguishable [39, 41, 42].

1.3.2 Retention or Stability. A memory device should have a long retention time (> 10 years) which determines the length of time that data can be stored inside the memory devices [2, 43-45].

1.3.3 Operating Voltage. Operating voltage in memory devices is an important parameter. A low operating voltage is favorable to have less power consumption and to avoid fatal damage during practical application [6, 26, 39, 46, 47].

1.4 RESISTANCE SWITCHING MECHANISMS

1.4.1 Conduction Mechanism in LRS. A clear understanding of resistance switching is necessary for future application of RRAM. Generally, the conduction mechanism in LRS can be categorized according to the conducting path; an interface-type conduction path and a filamentary conduction path [3, 6, 49, 50, 51].

Interface-type conduction path

In an interface-type conducting path, the resistance switching takes place over the entire area of interface between the metal electrode and oxide material [3, 6].

Different models have been suggested for an interface-type conducting path, including electrochemical migration of oxygen vacancies in the vicinity of the interface between an oxide and metal electrode, trapping/detrapping of charge carriers, and insulator-metal transition in which charge injection acts like doping at the interface [3, 40].

Filamentary conduction path

According to the filamentary mechanism, the formation and rupture of conductive filaments is responsible for switching the material between LRS and HRS [16, 34, 52-57]. Electromigration of cations/anions, redox reactions, and thermal effect are expected to be involved in the filament model [40, 58-61].

The electromigration of cations usually happens due to the diffusion of metal cations from an electrochemically active electrode into the insulator resulting in conductive path between the top and bottom electrodes [40]. When a positive voltage is applied to the electrochemically active metal electrode of cell, the following processes take place in resistance switching: oxidation of metal atoms to the metal cations; drift of highly mobile cations in the oxide layer; reduction of the cations at the inert metal electrode resulting in formation of conductive filaments (LRS of cell) in FORMING and SET process. In RESET process, when the polarity of applied voltage is reversed, the conductive filaments are partially dissolved leading to the HRS of the cell [6, 62].

Anion migration mostly takes place in transition metal oxides in which the oxygen ion defects such as oxygen vacancies are much more mobile than cations. Under an applied electric voltage and thermal effect, oxygen ions are retracted from the oxide material resulting in the formation of oxygen deficient region. Transition metal cations can accommodate this deficiency by redox reaction resulting in formation of metallic filaments [63-66].

1.4.2 Conduction Mechanism in HRS. Based on the current-voltage (I-V) relationships, some models have been proposed for conduction mechanism in HRS such as Space-Charge-Limited Conduction, Schottky emission, and Poole-Frenkel emission [39, 67, 68].

Space-Charge-Limited Conduction (SCLC)

One of the considered mechanisms for conduction behavior in the as-deposited state and HRS of resistance switching is Space Charge Limited Conduction (SCLC). Under an applied electric field, the charge injected by the electrodes exceeds the free carrier density in the insulating material resulting in SCLC [69]. In this mechanism, the current-voltage curve shows three different regions; Ohmic region ($I \propto V$), the Child's law region ($I \propto V^2$), and a region with a sharp current increase [5, 70]. The current for Child's law is [32, 69]

$$I = \frac{9\mu\varepsilon_0\varepsilon_i}{8L^3} AV^2 \qquad (1)$$

where μ is carrier mobility (cm^2.V^{-1}.s^{-1}), ε_o is permittivity of free space (F.cm^{-1}), ε_i is the dynamic dielectric constant, L is the thickness of the film (cm), A is the cross sectional area of top electrodes (cm^2), and V is the electrical voltage.

Schottky Emission

The second mechanism for conduction behavior in as-deposited and HRS is Schottky emission which is related to the metal-insulator interface [71]. The difference between the Fermi levels of a metal and an insulator creates a potential barrier which may be lowered under an applied electric field [72]. The emission of electrons over a reduced potential barrier results in Schottky emission and can be expressed as follows [71]:

$$I_S = \frac{4\pi q {k_B}^2 m^*}{h^3} A T^2 \exp\left(-\frac{\phi_B}{k_B T} + \frac{\sqrt{\frac{q^3 V}{4\pi L \varepsilon_o \varepsilon_i}}}{k_B T} \right) \quad (2)$$

where I_S is current in Schottky emission (C.s^{-1}), q is the electron charge (C), k_B is Boltzmann's constant (J.K^{-1}), m^* is the effective electron mass in the dielectric (Kg), h is the Planck's constant (J.s), T is the temperature (K), and ϕ_B is the Schottky barrier height (eV).

Poole-Frenkel Emission

The third conduction mechanism in the as-deposited state and HRS is Poole-Frenkel emission which is associated with the lowering of the trap barrier in the bulk of an insulating material under an applied electric field [71-73]. This lowering of the trap

barrier can increase the probability of excitation of electrons from the trap centers (most likely point defects) into the conduction band of a dielectric [73].

In Poole-Frenkel emission, the relationship between the current (I) and applied electric voltage (V) can be expressed as [71, 74]:

$$\frac{I}{V} = \frac{q\mu N_C}{L} A \exp\left(\frac{-\phi_t}{k_B T} + \frac{\sqrt{\frac{q^3 V}{\pi L \varepsilon_o \varepsilon_i}}}{k_B T} \right) \quad (3)$$

where N_C is the density of states in the conduction band (cm^{-3}), and ϕ_t is the trap energy barrier height in oxide films (eV).

1.5 LITERATURE REVIEW ON RESISTANCE SWITCHING OF METALLIC OXIDES

1.5.1 Resistance Switching of Cu_2O and CuO. The early work on resistance switching of oxides started in 1969 by Cook [75] who studied resistive-conductive behavior of Cu_2O and assumed a filamentary conduction mechanism for switching. The same assumption was made by Severdenko et al. [76] (1977); they produced Cu_2O thin films by anodization of Cu films in a potentiodynamic regime, and observed switching between HRS and LRS; they assumed the transition from HRS to LRS may be the result of a disproportionation of Cu_2O ($Cu_2O \rightarrow Cu + CuO$). These works did not provide any physical support to back up the assumption of formation of a Cu filament. Other works

suggested different switching mechanisms in Cu_2O. In 1973, Zarabi and Satyam [77] suggested that a purely electrothermal process could be the cause of switching in Cu_2O. In 2007, Chen et al. [78] suggested that the switching behavior in Cu_2O could be due to a charge trapping process. From the above works on switching behavior of Cu_2O, it is clear that the switching mechanism in Cu_2O is yet to be determined.

CuO also exhibits switching behavior. Lv et al. [8] studied the effect of the top electrode (Al, Ti, Pt) on the electrical properties of Cu-oxide based RRAM and they showed improvement of resistance ratio, stability, and endurance by using an Al electrode. They suggested that formation of AlO_x at the interface of Al and Cu-oxide controls the diffusion of oxygen ions out of metal electrode and improves the resistance switching performance. In 2009, Yasuhara et al. [27] studied the chemical states in resistance switching of Pt/CuO/Pt structure by photoemission electron microscopy (PEEM) and they suggested the conductive filament forms due to the Joule-heat-assisted reduction of CuO. In 2008, Fujiwara et al. [31] suggested that the resistance switching in CuO is due to the local redox reactions. Kim et al. [35] also suggested formation of conducting filaments in Pt/CuO/Au using impedance spectroscopy and conductive atomic force microscopy (CAFM).

During the last 10 years more research has been devoted to the study of switching behavior of different oxides. In the following paragraphs, the switching behavior of NiO, TiO_2, ZnO, and some other oxides is reviewed.

1.5.2 Resistance Switching of NiO. In 2007, Park et al. [79] studied the resistance switching of NiO_x. They showed that the grain structure of NiO_x changed after the forming process and Ni filaments formed along grain boundaries resulting in

switching the NiO_x to LRS. In 2008, Son and Shin [45] studied the resistance switching of NiO thin films by high-resolution conducting atomic force microscope (CAFM). They suggested that in HRS, the leakage current regions are almost located at grain boundaries while in LRS, filaments are formed at the grain boundary regions as well as non-grain boundary regions. Kim et al. [64] (2008) reported resistance switching in NiO nanowires and they showed that a lower electric field is required for electroforming of NiO nanowires compared to the NiO thin films. Park et al. [80] (2008) compared the resistive switching properties of two types of Pt/NiO/Pt structures with epitaxial and polycrystalline NiO layers. They reported unstable and poor reproducibility switching in epitaxial NiO films compared to the polycrystalline NiO films. This suggested that the microstructural defects such as grain boundaries play a crucial role in resistance switching of NiO films. Lee et al. [81] (2008) studied the effects of top metal electrodes (Pt, Ta, Al, Cu, and Ag) on resistance switching of NiO films. They showed repetitive resistance switching in Pt/NiO/Pt and loss of resistance switching after 24 hrs in Pt/NiO/Al and Pt/NiO/Ta. They suggested that the creation of metal oxide at the interface between metal electrodes (Ta and Al) and NiO affects the resistive switching due to the metal oxide breakdown that occurs at the anodic site. They also proposed that the migration of Cu and Ag atoms effect resistive switching of NiO films. In 2009, Lee et al. [82] showed formation of nanoscale conducting paths of Ni at the grain boundaries of NiO thin films by secondary-ion mass spectroscopy (SIM). In 2013, Jiang et al. [13] suggested formation of metallic filaments in NiO thin films using complex impedance spectroscopy.

1.5.3 Resistance Switching of TiO_2. In 2005, Choi et al. [17] studied the resistance switching of TiO_2 thin films. They showed formation and rupture of conducting filaments in resistance switching of TiO_2 by CAFM in high vacuum. They suggested that switching to LRS is due to the point defects alignment in bulk material. In 2007, Kim et al. [83] assumed that a conductive filament will form during switching, and based on this assumption they claimed the rupture and recovery of conductive filaments occur in the region near anode metal electrode (the electrode which is connected to the positive voltage source). They also suggested that in TiO_2 the electrical conduction in HRS is due to the space charge limited current mechanism. In 2008, Yang et al. [61] reported the bipolar switching in a $Pt/TiO_2/Pt$ cell. They claimed that the resistance switching involves changes to the electronic barrier at the Pt/TiO_2 interface due to the drift of positively charged oxygen vacancies under an applied electric field resulting in shunting the electronic barrier and switching the $Pt/TiO_2/Pt$ cell to the LRS. The drift of vacancies away from the interface recovers the electronic barrier and changes the resistance of the material to the HRS. In 2010, Kwon et al. [59] observed formation and disruption of Ti_nO_{2n-1} (Magneli phase) as conducting filaments in unipolar switching of TiO_2 by high-resolution transmission electron microscopy (TEM). They suggested that during the initial forming process oxygen atoms are displaced from the bulk position by external electric field and thermal effect resulting in the creation of random oxygen vacancies which will spontaneously rearrange to form an ordered structure. In 2010, Strachan et al. [66] also showed formation of Ti_4O_7 (Magneli phase) in bipolar switching of TiO_2 by scanning transmission x-ray microscopy (STXM) and TEM.

1.5.4 Resistance Switching of ZnO. In 2008, Xu et al. [49] studied the bipolar resistance switching of TiN/ZnO/Pt based resistance random access memory devices. They suggested generation/recovery of oxygen vacancies as the resistance switching mechanism in oxide RRAMs. In 2009, Yang et al. [5] developed a fully room temperature-fabricated Ag/ZnO:Mn/Pt device. They showed that formation and rupture of Ag bridges which is due to the redox reaction results in resistance switching of ZnO:Mn. In 2011, Zhuge et al. [84] reported an improvement in resistive switching properties of Cu/ZnO/Pt memory cells by doping ZnO with N at elevated temperature. They showed that N-doped ZnO films have larger grains with fewer grain boundaries, resulting in a depression of the randomness of the formation and rupture of Cu filaments. Additionally, they confirmed formation of nanoscale filaments at grain boundaries of ZnO by CAFM. In 2012, Tang et al. [32] studied the effect of the top electrode on resistance switching behavior of polycrystalline ZnO films deposited on a Pt/Ti/SiO_2/Si substrate. They observed unipolar resistance switching (URS) in Pt/ZnO/Pt and bipolar resistance switching (BRS) in Ag/ZnO/Pt structure devices. They suggested filamentary conduction mechanism in both URS and BRS. In 2012, Chiu et al. [19] reported BRS in a Pt/ZnO/Pt structure. They reported a high ac cycling endurance ($>10^6$ cycles) and a low dc cycling endurance (100 cycles) in their device structure. Based on the I-V measurements, they suggested hopping and ohmic conduction in HRS and LRS, respectively. In 2013, Younis et al. [85] reported improvement of the resistance switching behavior of pure ZnO by using Ti dopants. They explained the resistance switching mechanism by trap-controlled space-charge-limited conduction theory. In 2013, Huang et al. [50] studied the unipolar and bipolar switching in Pt/ZnO/Pt structure. They suggested

formation and rupture of metallic filaments by joule heating as the unipolar resistance switching mechanism and trapping-detrapping effect as the bipolar resistance switching mechanism. In 2013, Chen et al. [62] observed the formation and rupture of conductive filaments in Pt/ZnO/Pt structure via in situ transmission electron microscopy (TEM). They showed that the filament is composed of metallic zinc and they proposed an electrochemical redox reaction model to explain the resistive switching phenomena.

1.5.5 Resistance Switching of Other Oxides. In the literature, there are some works on resistance switching of other oxides, such as Nb_2O_5, $SrTiO_3$, and MoO_x. In 2005, Sim et al. [86] reported that the resistance switching mechanism in Nb_2O_5 is due to the semiconductor-to-metallic transition and filamentary conduction. They estimated degradation of the LRS and HRS at 125 ^{o}C for 10 years is approximately 8 percent indicating great potential of their device for nonvolatile memory application. They also explained the conduction mechanism in HRS by field-assisted Poole-Frenkel behavior.

In 2006, Szot et al. [24] studied the resistance switching behavior of a ternary oxide, $SrTiO_3$ and they suggested extended defects, such as dislocations, cause the resistance switching in single-crystalline $SrTiO_3$.

Lee et al. [87] reported reproducible resistance switching of Cu doped MoO_x for over 10^6 cycles under alternating voltage pulses. They used CAFM and showed localized high conductance spots after switching to LRS. Based on this result, they suggested formation of multi filaments in Cu doped MoO_x. In 2008, Ahn et al. [48] improved the performance of RRAM unit cells by combination of Ti doping in NiO and small cell sizes patterned using a cross-bar architecture. They reported a very low writing current (current in LRS) of 10 μA and a programming speed of 10 ns.

1.6 PROCESSING METHODS AND PROPERTIES OF CUPROUS OXIDE

Different techniques can be used to grow cuprous oxide films, such as chemical vapor deposition, thermal oxidation of copper, and electrodeposition [88-90]. Electrodeposition has advantages of low cost, low operating temperature, and provides high purity thin films [91].

Cuprous oxide is a p-type semiconductor with a direct band gap of 2.0 eV [42] which has been used in solar energy conversion, catalysis, and as active sensor platforms because of its low-cost preparation and non-toxicity [88]. Recently, this material has received attention due to its potential application in resistance switching random access memory (RRAM) [88, 92, 93].

From Sub-section 1.5.1 on the switching behavior of Cu_2O, it is clear that the switching mechanism in Cu_2O is yet to be determined, and more work needs to be done to identify the parameters controlling the switching in Cu_2O and also determine some physical evidence explaining the switching mechanism. This research project was aimed to methodically study the switching mechanism in Cu_2O.

2. RESEARCH OBJECTIVES AND IMPACTS

The overall goal of this work is to study the resistance switching properties of cuprous oxide and determine the parameters controlling the switching behavior. Electrodeposition is used to produce cuprous oxide thin films, and a series of experiments, including current-voltage measurements and ac-impedance spectroscopy, are performed to determine electrical properties of each state of resistance switching in the electrodeposited cuprous oxide. The objectives of this research project are outlined below.

- Objective 1: Study the resistance switching properties and the performance parameters (e.g., endurance and stability) of electrodeposited cuprous oxide thin films by dc current-voltage curve measurements.
- Objective 2: Investigate the physical property of material in each state of resistance switching process by ac-impedance spectroscopy and resistance vs. temperature plots.
- Objective 3: Study the effect of different parameters such as microstructure and thickness of electrodeposited cuprous oxide thin films, compliance current, top electrode area, and top electrode material on resistance switching of cuprous oxide thin films.
- Objective 4: Study the scalability and switching mechanism of Pt/Cu_2O/Pt device structure by producing Cu_2O nanowires and depositing Pt top and bottom electrodes using an electron beam.

The results of this work may help electronic industries to improve the RRAM device characteristics and provide guidelines to obtain low power consumption, high scalable and high density memory device. Different experiments were performed in this work to gain fundamental understanding of resistance switching mechanism which is necessary for practical application of RRAM.

PAPER

I. COPPER NANOFILAMENT FORMATION DURING UNIPOLAR RESISTANCE SWITCHING OF ELECTRODEPOSITED CUPROUS OXIDE

This paper has been submitted to *CHEMISTRY OF MATERIALS*

Sanaz Yazdanparast,[1] Jakub A. Koza,[2] and Jay A. Switzer[1,2*]

[1]Department of Materials Science and Engineering, Missouri University of Science and Technology, Rolla, Missouri, 65409-1170, United States

[2]Department of Chemistry and Graduate Center for Materials Research, Missouri University of Science and Technology, Rolla, Missouri, 65409-1170, United States

ABSTRACT

An emerging non-volatile, solid-state memory is resistance switching random access memory (RRAM). RRAM is based on reversible switching of resistance in semiconductor and insulator thin films. Here, unipolar resistance switching is demonstrated in electrodeposited films of [111]-textured cuprous oxide (Cu_2O). The textured cuprous oxide is electrodeposited from a highly-alkaline bath using tartrate as the complexing agent. The switching is observed in a cell composed of a film of Cu_2O sandwiched between Au and Au-Pd contacts. The switching is attributed to the formation and rupture of a Cu nanofilament in the Cu_2O. The initial resistance of the cell is 6.17 x 10^6 Ω, and a conducting filament is formed in the film by scanning the applied electric field to 6.8 x 10^6 V/m. The cell is then reversibly cycled between a low resistance state of 16.6 Ω and a high resistance state of 0.4 x 10^6 Ω by SET and RESET processes. In the low resistance state the resistance decreases linearly with decreasing temperature, consistent with metallic behavior. The resistance temperature coefficient of 1.57 x 10^{-3} K^{-1} is similar to that of nanoscale metallic Cu. Current-voltage (I-V) data suggests that applying a higher compliance current increases the filament size during the FORMING and the SET process, and also causes a higher RESET current. The calculated filament diameter varies from 50 to 147 nm for compliance currents ranging from 10 to 100 mA. At high electric voltage in the as-deposited state, the conduction behavior follows Poole-Frenkel emission. The filament temperature is estimated from the non-ohmic behavior of the cell in the RESET step. The calculated temperature of 798 K before rupture of the Cu filament suggests Joule heating of the filament, resulting in melting, sintering, or thermal oxidation of Cu filament.

KEYWRODS

Electrodeposition; unipolar resistance switching; cuprous oxide; nanofilament; Joule heating.

INTRODUCTION

Nonvolatile memory is widely used in different electronic applications because of its ability to store data even if the power is removed [4]. Among several types of nonvolatile memories [3, 7, 41], resistance switching random access memory (RRAM) has attracted recent attention because of its reversible switching, scalability, low power consumption, and low cost [2, 93, 94]. An RRAM cell is composed of an insulating or semiconducting material sandwiched between two metal electrodes [95]. There are various types of materials (e.g. perovskites and chalcogenides) that show resistance switching behavior [1, 12, 17, 24, 40, 65, 96, 97], and among them binary oxides such as Cu_2O, NiO, and TiO_2 are receiving increasing interest due to their simple composition, thermal stability, and compatibility with complementary metal–oxide-semiconductor (CMOS) technology [5, 21, 22].

A crucial characteristic of RRAM is the soft dielectric breakdown of insulating or semiconducting materials that causes a reversible switching from a high resistance state (HRS) to a low resistance state (LRS) [14, 59, 83]. Soft dielectric breakdown is assured by applying an appropriate compliance current. Based on the polarity of voltages required for changing the HRS to the LRS (SET) and vice versa (RESET), resistance switching can be classified as either unipolar and bipolar switching [80]. In unipolar switching, the

SET and RESET processes are dependent on the values of applied voltage, whereas in bipolar switching they are dependent on the voltage polarity [34, 98].

Several mechanisms have been proposed for resistance switching [31, 45], and among them the filamentary mechanism (formation of a conductive filament) has been widely accepted in transition metal oxides [42, 83, 99]. However, the physical properties of these filaments, the rupture mechanism, and also the effect of various important parameters such as the compliance current in resistance switching process is not fully understood.

Unipolar resistance switching behavior of electrodeposited cuprous oxide thin films was shown previously by Kang et al. [88] The as-deposited cuprous oxide prepared by their work did not show resistance switching before an additional rapid-thermal-annealing treatment. In this work, we report unipolar resistance switching of as-deposited, textured films of cuprous oxide prepared by electrodeposition. We studied the effect of compliance current on the RESET parameters, the rupture mechanism of resistance switching, and the physical properties of the material in each state of resistance switching process. We show that the switching mechanism is consistent with the formation and rupture of a nanoscale metallic Cu filament, and that the filament diameter can be controlled by varying the compliance current.

EXPERIMENTAL

Cuprous oxide thin films with 5 μm and 2 μm thicknesses were electrodeposited cathodically onto gold coated glass substrates (SiO_2/30 nm Ti/100 nm Au). The electrodeposition process was performed at a constant current density of 1 mA/cm^2 and

60° C using Cu(II) tartrate solution; 0.2 M L(+)-tartaric acid, 0.2 M copper (II) sulfate pentahydrate, and 3 M sodium hydroxide [90]. The structure and orientation of Cu_2O thin films was identified by a high resolution Philips X-Pert MRD X-ray diffractometer (XRD) using Cu Kα radiation (wavelength of 1.54056 Å) at 45 kV and 40mA. The surface morphology of the thin films was characterized with scanning electron microscope (SEM).

In order to measure the resistance switching behavior of the cuprous oxide thin films, circular Au-Pd top electrodes with a diameter of 260 μm and a thickness of 100 nm were sputtered on the films using a shadow mask. Electrical connection to the top electrodes was performed by using a sharp Au spring pin contact. DC current-voltage properties were measured in air using a Keithley 2400 current source. The electrical property of different states of cuprous oxide was examined by AC-impedance spectroscopy (Solartron SI frequency response analyzer). Impedance properties were measured as a function of frequency from 100 mHz to 1 MHz. The as-deposited, low resistance and high resistance states of cuprous oxide thin films were measured by applying AC voltages of 1 V, 10 mV, and 50 mV, respectively.

The physical properties in the low resistance state (LRS) was determined using a Quantum Design Physical Property Measurement System (PPMS). Temperature dependence measurements of the resistance were carried out with pressed In contacts on cuprous oxide thin films instead of Au-Pd contacts which were used during DC and AC measurements. The high and low resistance states were measured at 5 nA, and 25 μA, respectively.

RESULTS AND DISCUSSION

CUPROUS OXIDE THIN FILMS. Cuprous oxide thin films were electrodeposited onto gold-coated glass substrates (SiO_2/30 nm Ti/100 nm Au) from a highly alkaline tartrate bath. The film deposits with 100% current efficiency from this solution, growing 1.2 μm for every 1 C/cm^2 of charge that is passed. Figure 1 shows the x-ray diffraction pattern (XRD) of electrodeposited a cuprous oxide thin film with a thickness of 5 μm. The XRD shows a highly [111]-oriented cuprous oxide film. Only the (111) and (222) reflections for Cu_2O are observed in the diffraction pattern. The [111] texture is a result of both the [111] texture of the sputtered Au substrate, and the [111] preferred growth direction in the alkaline tartrate bath.[31] The [111] texture of the film is also evident in the (110) pole figure that is shown in Figure 2. The pole figure shows a ring of intensity at a tilt angle of 36°, in good agreement with the expected 35.2^o angle between the [111] and [110] directions in the primitive cubic cuprous oxide structure. The ring indicates that the film has a [111] out-of-plane fiber texture, with no in-plane order. From the SEM image in Figure 3, it can be seen that large, flat grains of cuprous oxide were grown on the substrate by the electrodeposition process. The electrodeposited Cu_2O film offers essentially single-crystal grains in the perpendicular direction for resistance switching experiments, with no or minimal grain boundaries in the current path.

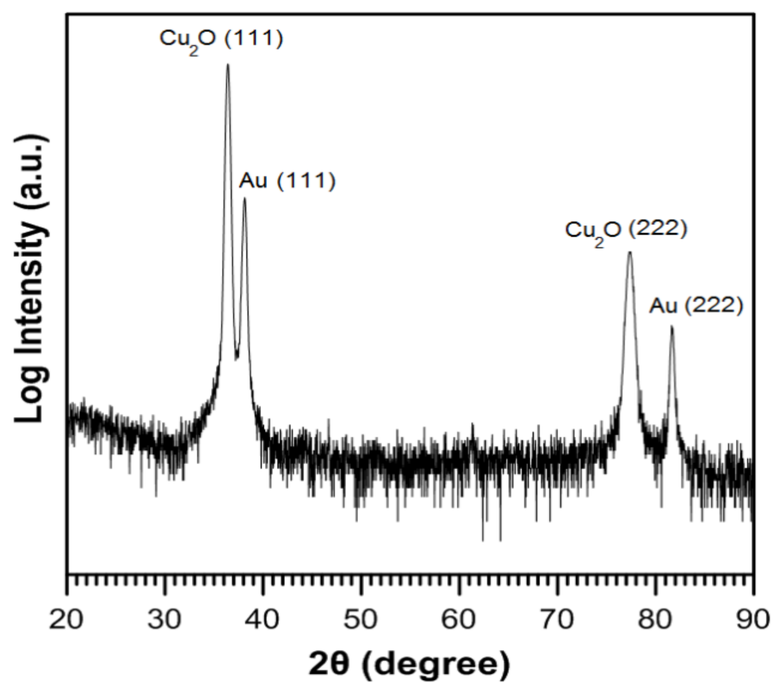

Figure 1. XRD pattern of electrodeposited cuprous oxide thin film (5 µm in thickness) on gold coated glass substrate.

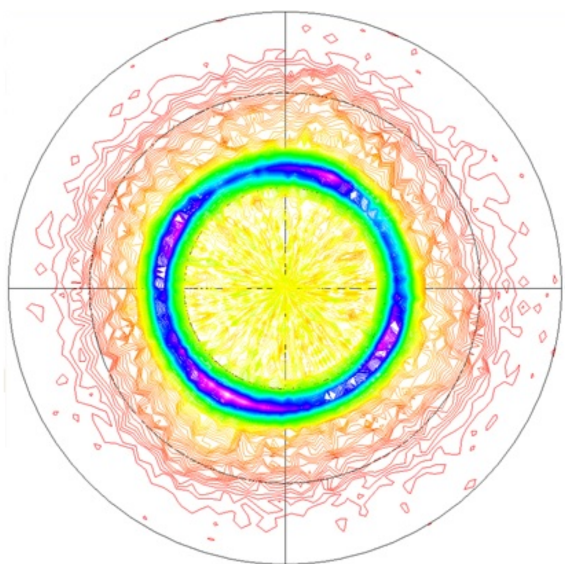

Figure 2. X-ray pole figure of [111]-oriented cuprous oxide on Au-coated glass. The (110) pole figure has a ring at a tilt angle of 36°, consistent with the [111] out-of-plane texture.

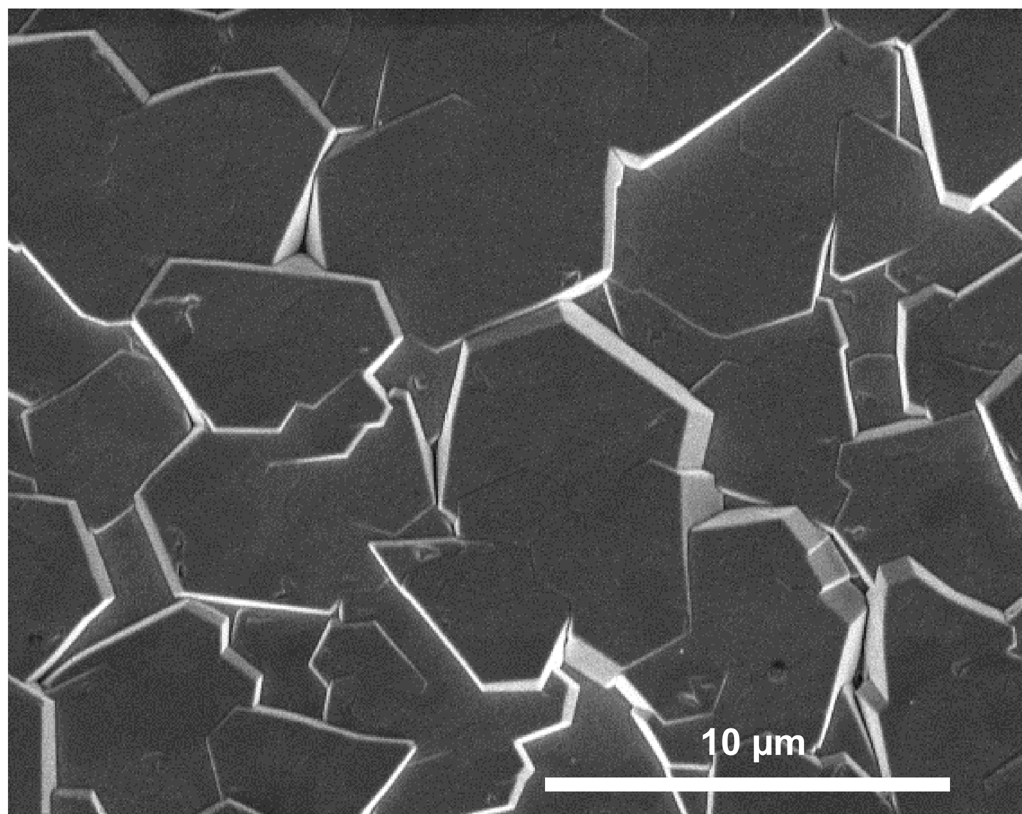

Figure 3. Top-view SEM image of cuprous oxide grains in a 5 µm thick film.

DC AND AC CHARACTERISTICS OF AS-DEPOSITED CUPROUS OXIDE THIN FILMS. The as-deposited cuprous oxide thin films show resistance switching behavior. During resistance switching measurements, a positive bias voltage was applied to the top electrode while the bottom electrode was grounded, as shown in Figure 4. DC current-voltage curve measurements of the electrodeposited cuprous oxide thin films show unipolar resistance switching (Figure 5). As it is shown in Figure 5a and 5b, the resistance switching process can be divided into 3 main steps; FORMING, RESET, and SET steps. During the FORMING step, a high voltage (34±6.7 V) with a compliance current (10 mA) is applied to the top electrode to switch the Cu_2O from its as-deposited state to the low resistance state (LRS). This bias corresponds to an electric

field of 6.8 x 10^6 V/m. According to the filamentary mechanism, a temporary conductive filament forms in the FORMING step which plays a crucial role in the reversible switching process. During the RESET and SET steps, rupture and reformation of the filament causes the reversible switching between high resistance state (HRS) and low resistance state (LRS) (Figure 4, bottom). The solid points in Figures 5 correspond to the average switching parameters of 5 different contact points with their standard deviation.

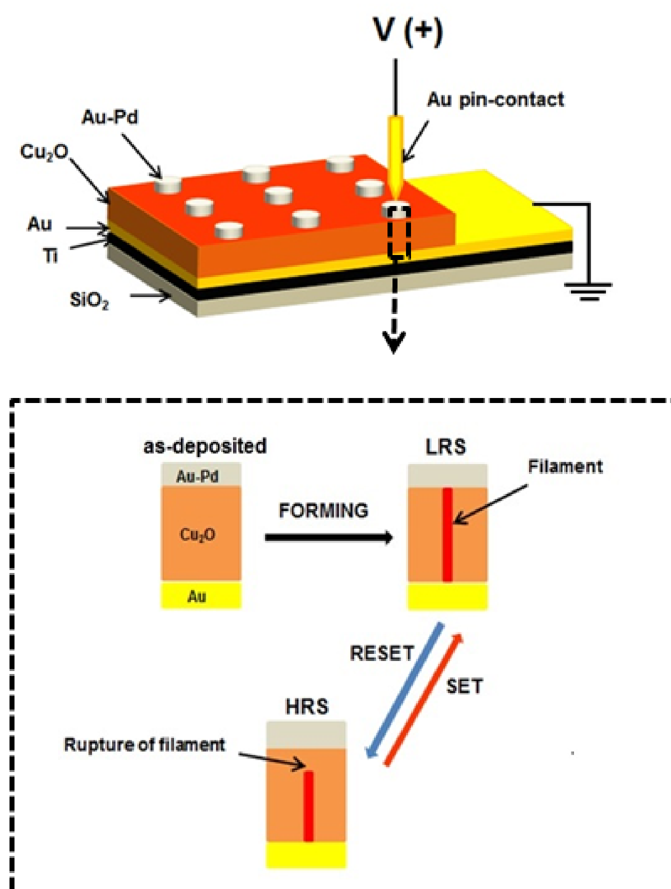

Figure 4. Schematic of resistance switching cell.

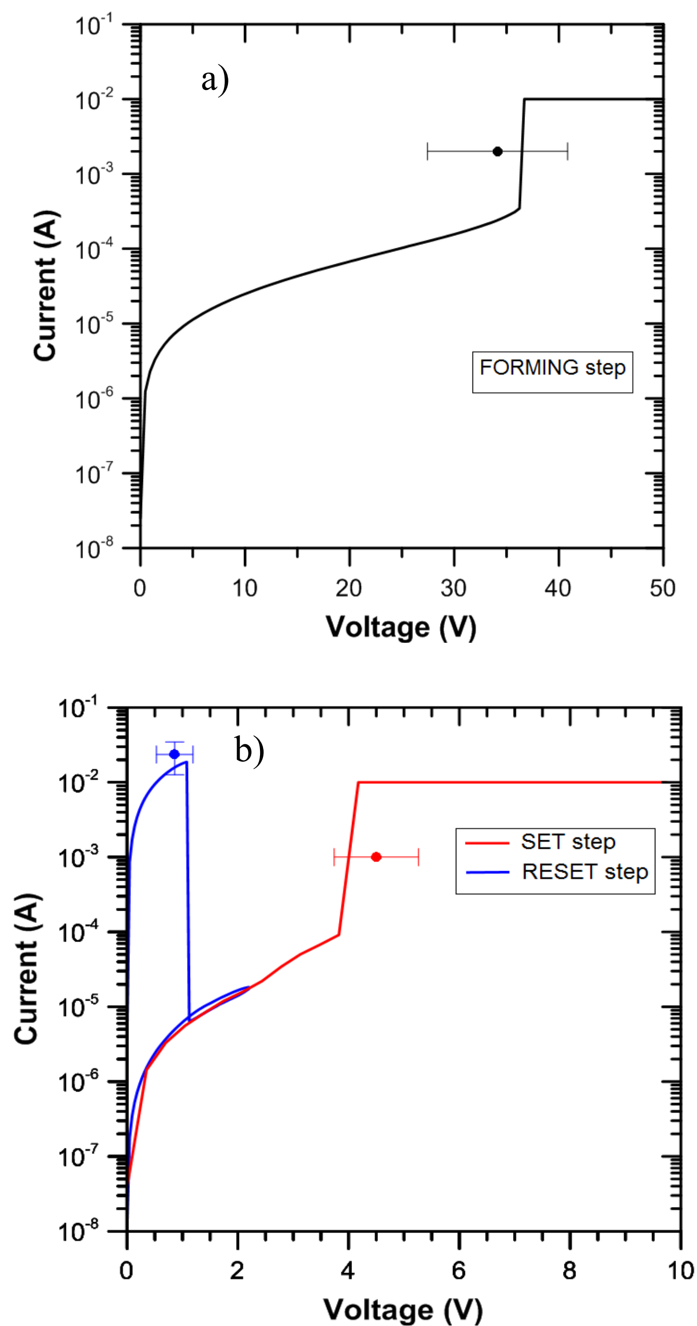

Figure 5. Current-voltage characteristic of Au/Cu_2O (5 μm in thickness)/Au-Pd cell during a) FORMING, b) RESET (blue) and SET (red) steps. Both FORMING and SET steps were performed at a compliance current of 10 mA. The scan rates of the RESET and SET steps were 0.68 V/s and 6.3 V/s, respectively. The solid points show the average values for switching parameters of 5 different contact points with their standard deviations.

Figure 6 shows the endurance property of Au/Cu_2O (5 μm thick)/Au-Pd cell. The reversible resistance states are stable for 170 cycles with a high resistance ratio (R_{HRS}/ R_{LRS}) of about 10^4. The stability of HRS and LRS versus time is shown in Figure 7. There is no significant change in both HRS and LRS during the retention test. The results from endurance and retention tests indicate the potential application of Au/Cu_2O/Au-Pd cell as a nonvolatile memory. The resistance values in both endurance and retention tests were measured at 0.025 V.

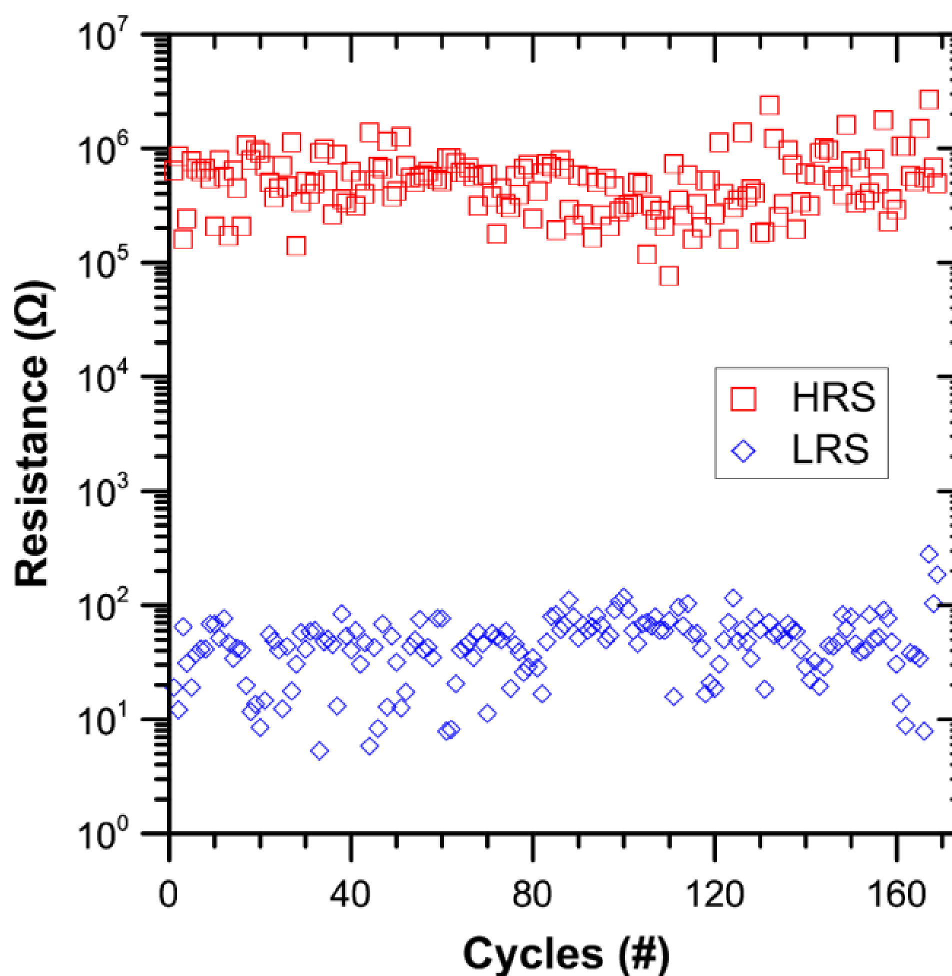

Figure 6. Endurance of the Au/Cu_2O (5 μm thick)/Au-Pd cell showing 170 cycles of stable reversible switching between LRS and HRS.

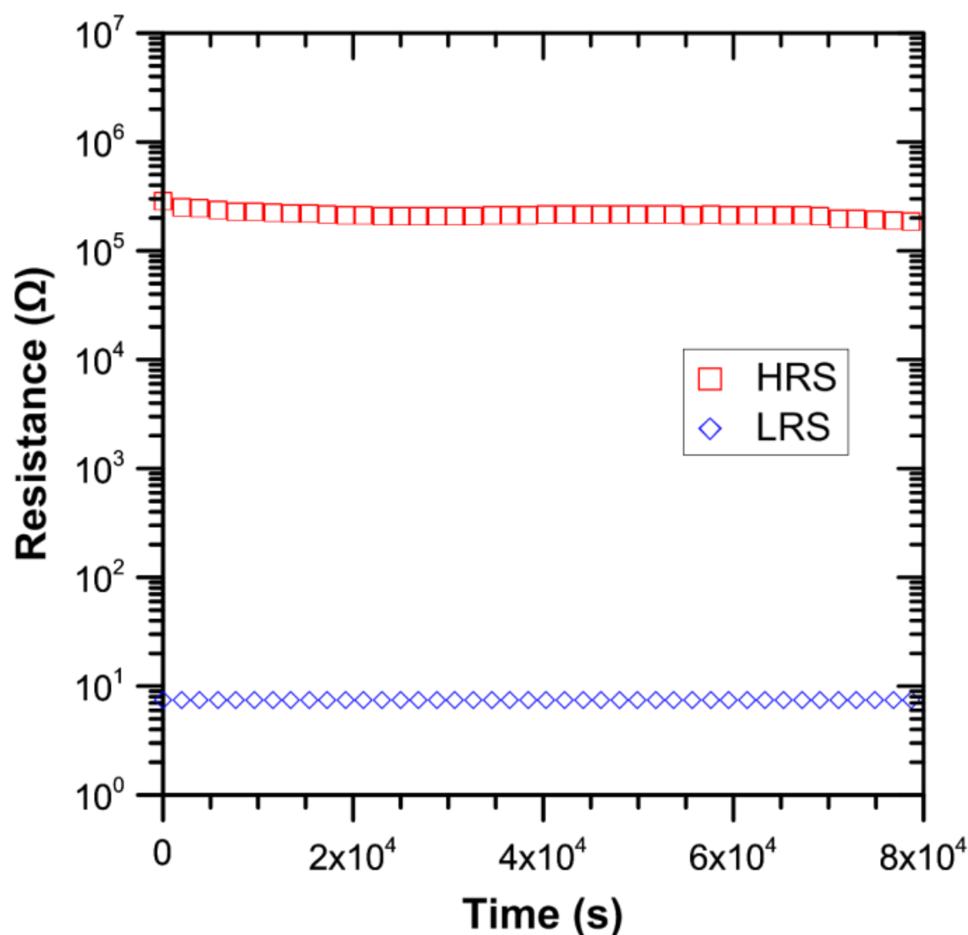

Figure 7. Retention characteristics of Au/Cu_2O(5 μm in thickness)/Au-Pd cell in each state of LRS and HRS. The resistance values in both HRS and LRS were measured at 0.025 V.

In addition to DC current-voltage properties, AC impedance spectroscopy was employed to determine the electrical property of the material in each state of the resistance switching process. Figures 8a and 8b show the Nyquist plots of the as-deposited, high, and low resistance states. The equivalent circuits of both as-deposited and high resistance states are composed of a parallel connection of a constant phase element and a resistor while in the low resistance state it consists of an inductor which is in series with a resistor. Different electrical properties of HRS and LRS indicate the metallic behavior of the filament in LRS and semiconductor behavior of the material in

HRS [13, 35]. The equivalent circuit parameters shown as insets in Figures 8a and 8b are summarized in Table I. A sharp decrease and increase of the resistance happens after the FORMING and RESET processes, respectively. Comparing the resistance values of both as-deposited state and HRS shows a decrease of resistance in HRS which can be due to the formation of a gap in the filament with a smaller thickness compare to the initial thickness of cuprous oxide [100]. Based on the information that we have about the cell such as contact area, the thickness of the film and resistance of the as-deposited state, the calculated resistivity of cuprous oxide is 3.8×10^{6} Ω.cm which is in good agreement with the reported value for resistivity of electrodeposited cuprous oxide [101, 102].

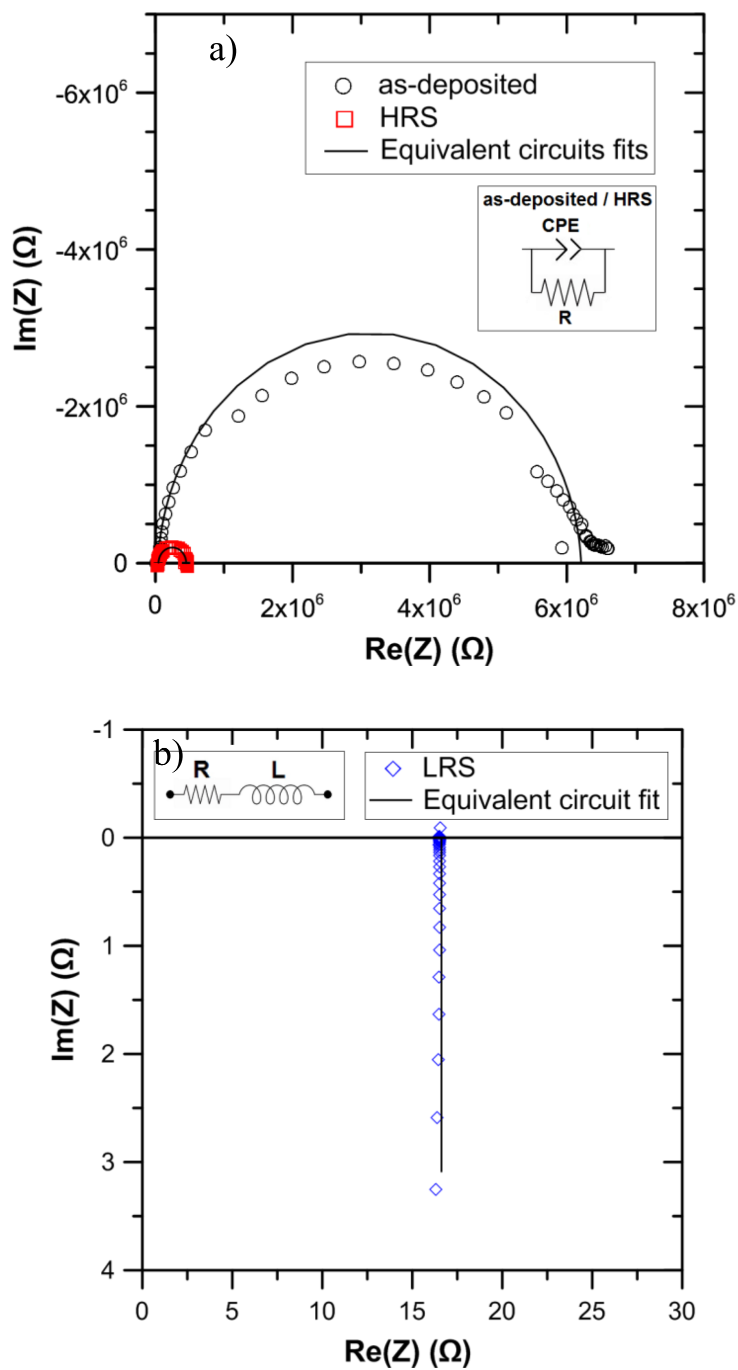

Figure 8. Impedance spectra of three different states of Au/Cu_2O (5 μm thick)/Au-Pd cell. a) as-deposited state (black circle), HRS (red square), and b) LRS (blue diamond) with their equivalent circuit fits. LRS was achieved by applying a compliance current of 10 mA.

Table 1. Summary of equivalent circuit parameters obtained from impedance spectroscopy at three different states.

	As-deposited state	LRS	HRS
R (Ω)	6.17×10^{6}	16.6	0.4×10^{6}
CPE (F)	1.93×10^{-11}	_	2.26×10^{-11}

FORMATION OF COPPER NANOFILAMENT IN RESISTANCE SWITCHING OF Cu_2O. The physical property of the material in each state of resistance switching process can be determined by measuring the resistance as a function of temperature (Figures 9 and 10). The measurements were made with an Au/Cu_2O (2 µm thick)/In cell. As shown in Figure 9a, the resistance of both as-deposited state and HRS increases exponentially by decreasing the temperature which shows semiconductor behavior of the material in these two states. Figure 9b shows the Arrhenius plot of the as-deposited state and HRS. From the Arrhenius plot, the activation energies for the as-deposited and HRS are 0.37 eV and 0.24 eV, respectively. These low activation energies may correspond to the energy difference of the valence band and the acceptor level of cuprous oxide which is a p-type semiconductor.

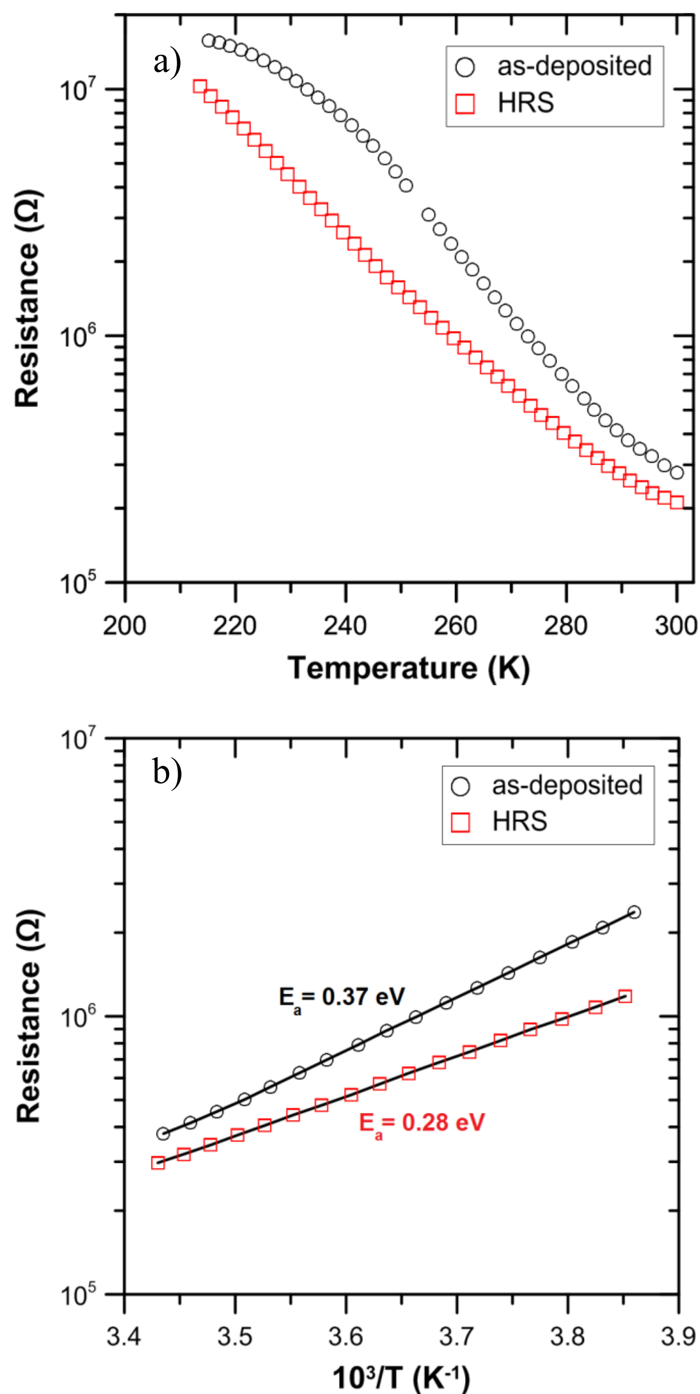

Figure 9. a) Resistance vs. temperature plots of the Au/Cu_2O (2 μm thick)/In cell in as-deposited state (black circle) and HRS (red square). b) The Arrhenius plots of the as-deposited state and HRS. The obtained activation energies of the Arrhenius plot for the as-deposited and HRS are 0.37 eV and 0.24 eV, respectively.

The resistance vs. temperature plot for the LRS is shown in Figure 10. The resistance decreases linearly when the temperature decreases from 300 K to 3.7 K. This result confirms the metallic nature of the filament in the LRS. From the fitted line, the slope of the resistance vs. temperature is 0.014 $\Omega.K^{-1}$ corresponding to a resistance temperature coefficient (α) of 1.57×10^{-3} K^{-1} at room temperature. This result is in reasonable agreement with the resistance temperature coefficient of Cu nanowires reported by Huang et al ($\alpha = 1.34\times10^{-3}$ K^{-1}) [103].

Assuming a cylindrical shape for the Cu filament allows us to calculate its diameter (d) by

$$d = \sqrt{\frac{4\rho L}{\pi R}}, \qquad (1)$$

where, ρ is the resistivity (Ω.m), L is the thickness of cuprous oxide (m), and R is the resistance of the filament (Ω). At room temperature ($T_0 = 300$ K), by assuming the resistivity of the bulk copper ($\rho = 1.71\times10^{-8}$ Ω.m [104]), and using the resistance of filament from Figure 10 ($R_0 = 8.8$ Ω; resistance at room temperature), the estimated diameter of a 2µm-long Cu filament is 70 nm. The resistivity is size dependent in the nanoscale range [105], and we expect a higher value of resistivity for a Cu nano-filament compared to bulk copper [103, 106] which will result in a larger diameter for the Cu filament by a factor of 1.5.

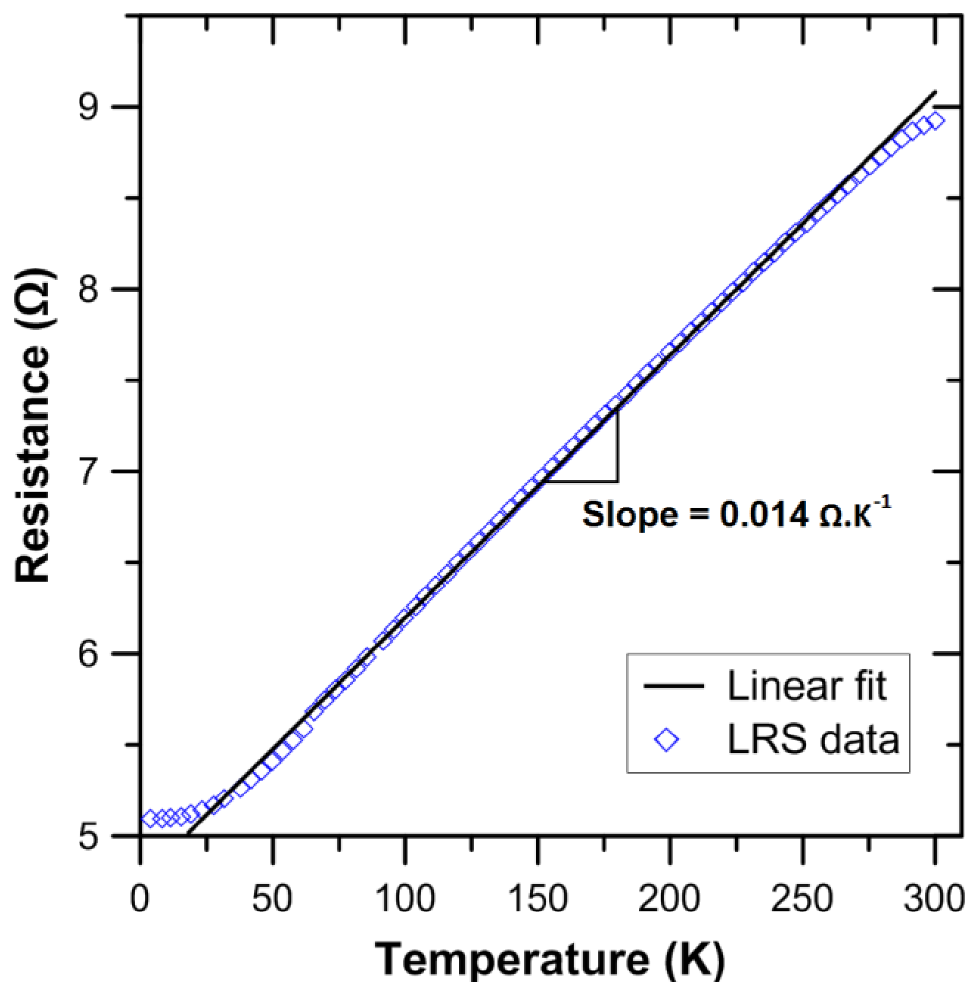

Figure 10. Resistance vs. temperature plot of the Au/Cu_2O (2 μm thick)/In cell in LRS with its linear fit. SET step was performed at compliance current of 25 mA.

In Figure 11, the effect of compliance current on the diameter of Cu filament is shown for a cuprous oxide with a thickness of 5 μm. For these calculations, the resistivity of bulk copper at room temperature was used, and the resistance value for each case was measured from the slope ($\partial I/\partial V = 1/R$) at the beginning part of its RESET plot (Figure 12). As it is shown in Figure 11, applying higher compliance current forms larger diameter filaments. The diameters of the copper filament are in the range of 50.5±16 nm to 146.9±6.8 nm at compliance currents of 10 mA to 100

mA. The filament's cross-sectional area plays a crucial role on reversible switching process, and a larger diameter of filament may result in permanent dielectric breakdown of oxide material.

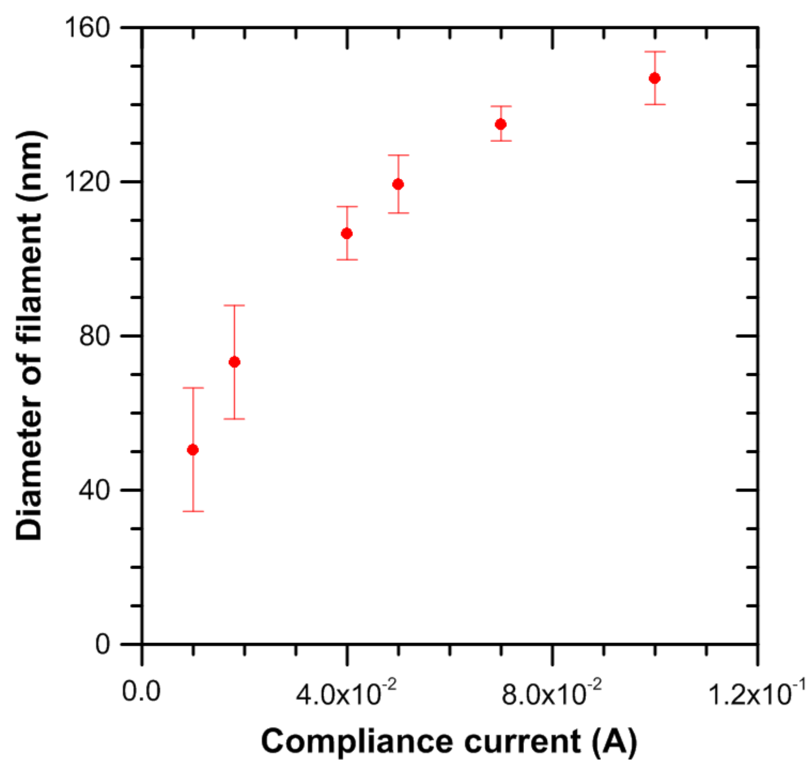

Figure 11. Diameter of the filament vs. compliance current in Au/Cu_2O(5 μm thick)/Au-Pd cell showing increasing the filament's diameter by increasing the compliance current. The solid points show the average diameter of filament for 5 different contacts with their standard deviations.

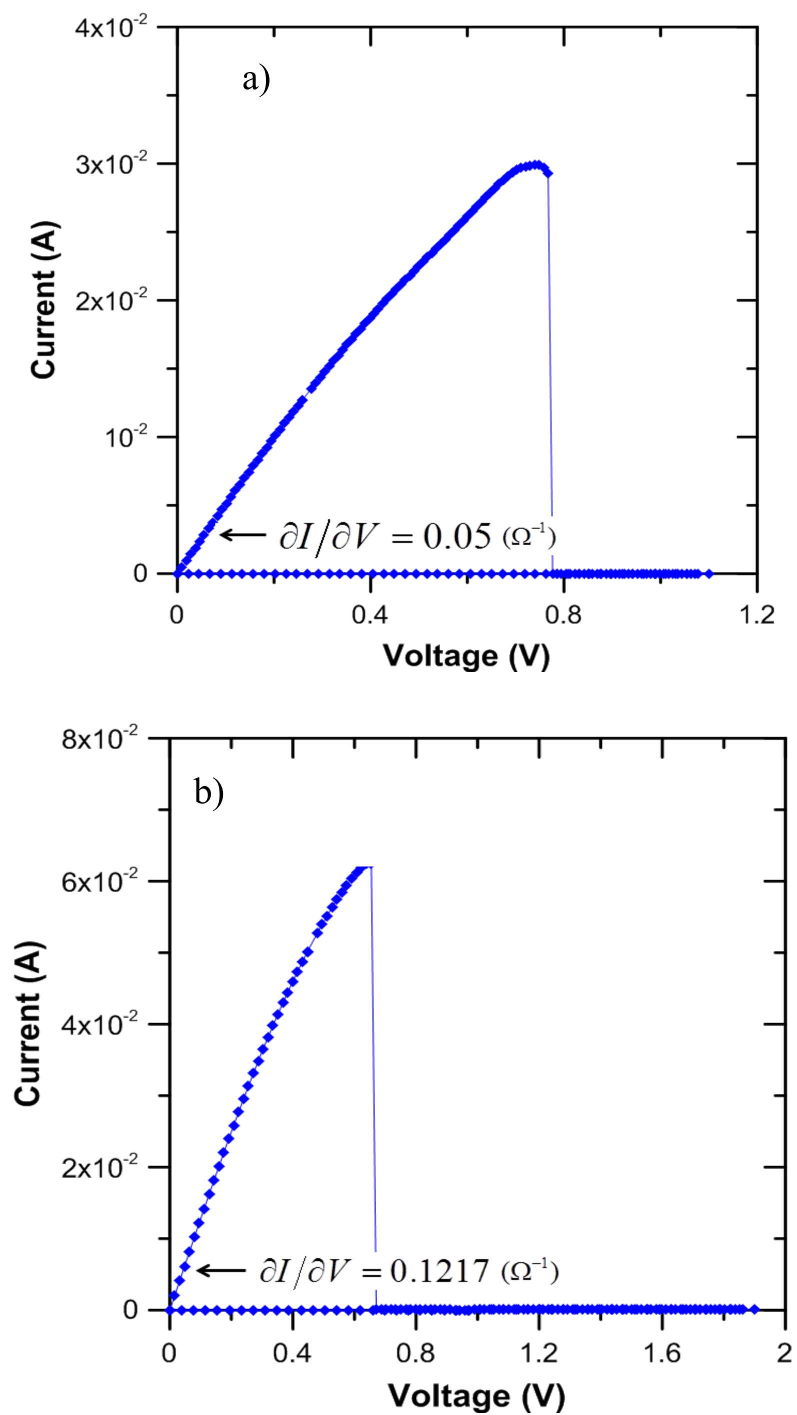

Figure 12. Corresponding RESET plots of Cu filaments with diameter of a) 73.7 nm which was formed at compliance current of 18 mA, and b) 115 nm which was formed at compliance current of 50 mA.

The effects of compliance current on RESET current, voltage, and current density was also studied. Figure 13 shows that the RESET current increases by increasing compliance current, while the RESET voltage is independent of compliance current (Figure 14). From these results, it can be inferred that the RESET current has a more significant effect in rupturing the filament compared to the RESET voltage. The amount of RESET current is proportional to the filament's diameter, and higher amount of current passes through a bigger filament. The current density can be estimated by using the calculated filament's diameter and the current flow ($j = 4I/\pi d^2$). The current density is almost independent of the compliance current and the average current density is estimated to be about 8.2±2.3 $\times 10^8$ A/cm^2 during RESET process (Figure 14).

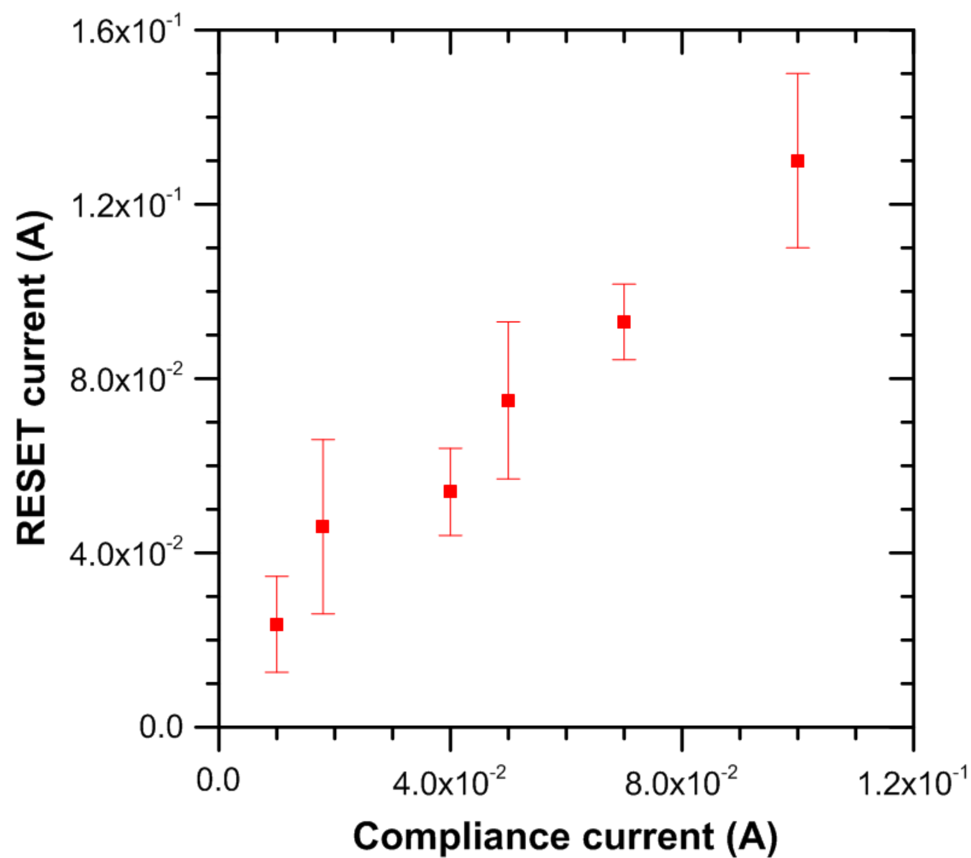

Figure 13. The effect of compliance current on RESET current in Au/Cu_2O (5 µm in thickness)/Au-Pd cell. The solid points show the average RESET current of 5 different contacts with their standard deviations.

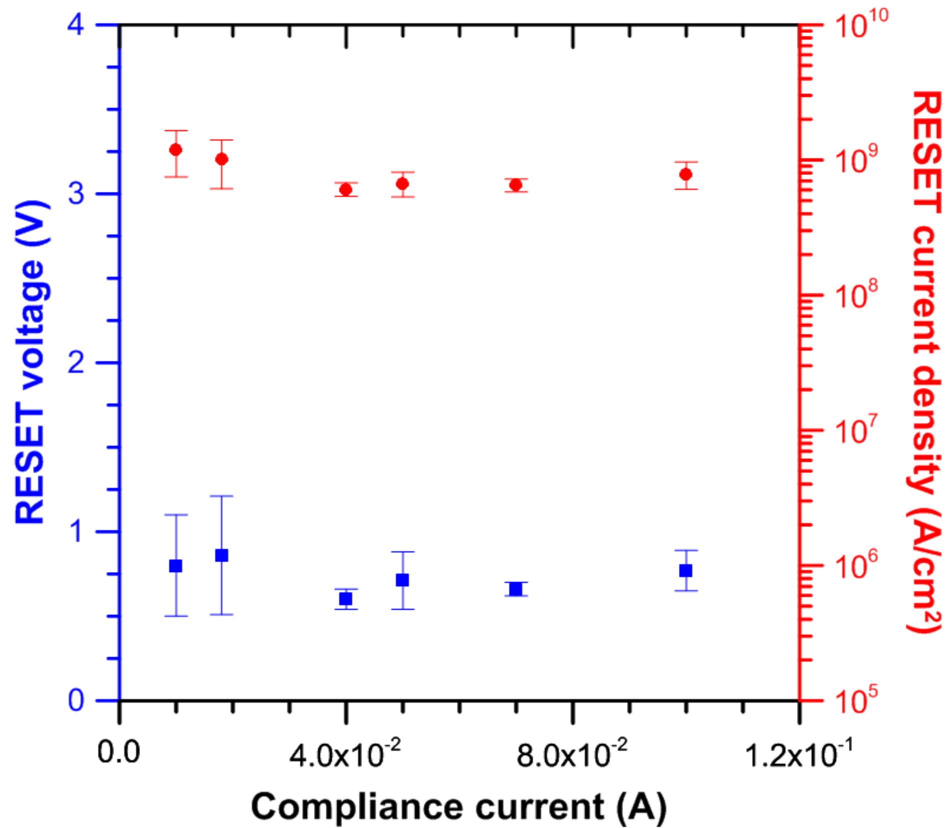

Figure 14. The effect of compliance current on RESET voltage (blue) and current density (red) in Au/Cu_2O (5 µm in thickness)/Au-Pd cell. The solid points show the average values of 5 different contacts with their standard deviations.

STUDYING THE RESISTANCE SWITCHING MECHANISM OF Cu_2O.

Despite various studies on resistance switching of different materials [45], the resistance switching mechanism is still unclear. To clarify this issue, certain relationships between current and voltage in each state of resistance switching can be used. Figure 15 shows the log I-log V of FORMING process. Different mechanisms are dominated in as-deposited state due to the different slopes of I-V curve. At low electric voltage, the conduction behavior follows Ohm's law which can be due to the electron hopping between the states of cuprous oxide with low activation energy [67]. In high electric

voltage (14.3-19.4 V), a non-linear behavior of log I-log V appears in as-deposited state of material which can be explained by Poole-Frenkel emission theory. According to the Poole-Frenkel emission [74], the relation between the current (I) and voltage (V) can be written as

$$\frac{I}{V}=\frac{q\mu N_C}{L}A\exp\left(-\frac{\phi_t}{k_BT}+\frac{\sqrt{\frac{q^3V}{\pi L\varepsilon_o\varepsilon_i}}}{k_BT}\right) \qquad (2)$$

where q is the electric charge (C), μ is the electronic mobility (cm^2.V^{-1}.s^{-1}), N_C is the density of states in conduction band (cm^{-3}), A is the cross sectional area of top electrode (cm^2), L is the thickness of the film (cm), ϕ_t is the trap energy barrier height in Cu_2O films (eV), k_B is the Boltzmann's constant, T is the temperature, ε_o is permittivity of free space (F.cm^{-1}), and ε_i is the dynamic dielectric constant. From the slope of $Ln\left(\frac{I}{V}\right)$ versus $V^{0.5}$ plot in the as-deposited state (Figure 16), the calculated dynamic dielectric constant is 6.5, which is close to the reported value of 6.6 for cuprous oxide [107]. Therefore, at high electric voltage the conduction mechanism in as-deposited state is dominated by Poole-Frenkel emission in which the high electric voltage causes thermal excitation of trapped electrons into the conduction band [67]. The electron traps are most likely point defects in the oxide films[108]. In the RESET process, a large current density is involved ($8.2\pm2.3\times10^8$ A/cm^2) which can result in Joule heating of the filament.

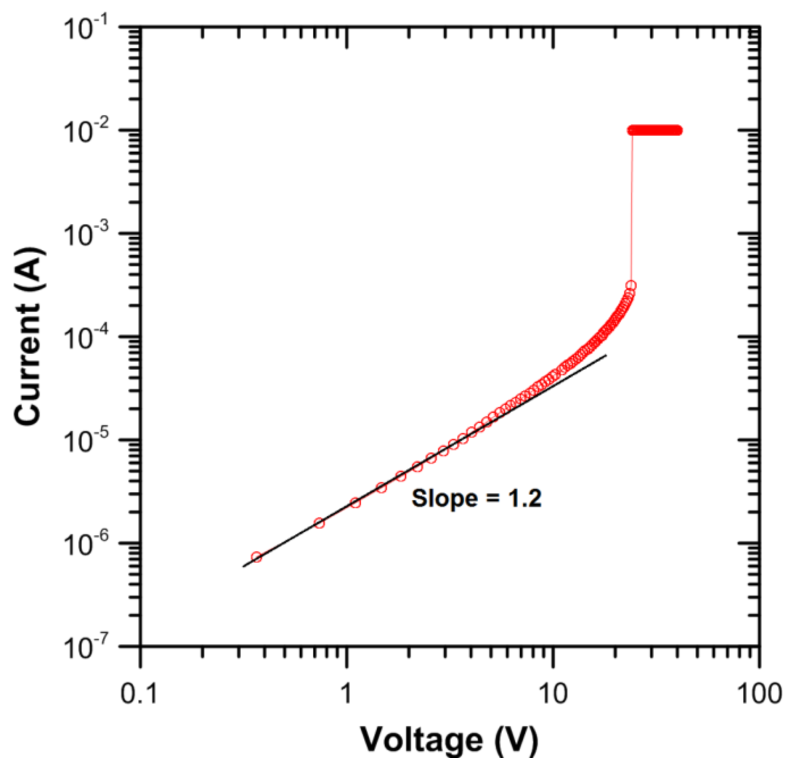

Figure 15. Log I-Log V curve of FORMING process showing linear and non-linear behavior at low and high electric voltage, respectively.

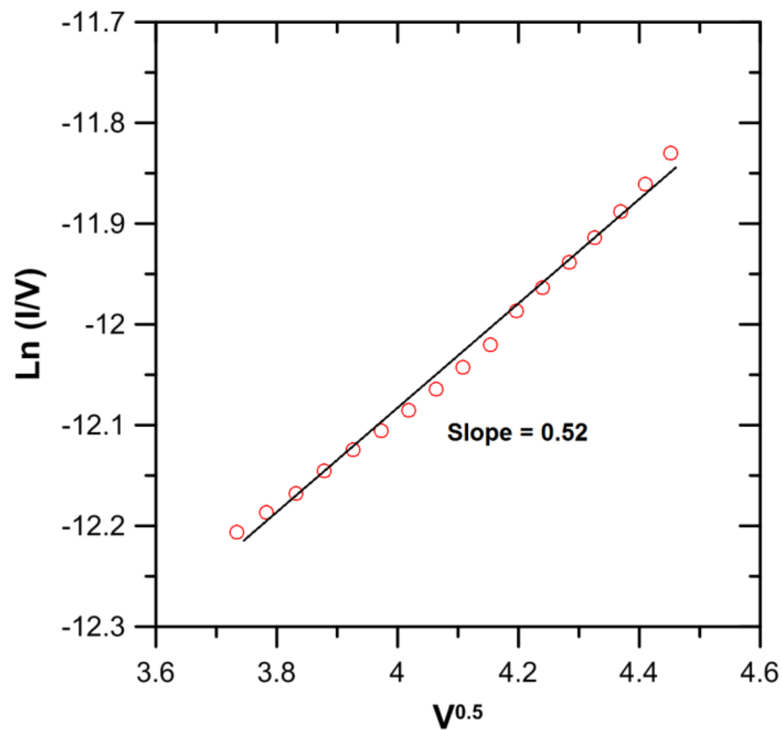

Figure 16. Poole-Frenkel emission plot of as-deposited state at high electrical voltage (14.3-19.4 V).

To understand the rupture mechanism, we estimated the temperature of the filament before rupturing by using the I-V curve of the RESET process. The data in our RESET curve show non-linear behavior resulting in change of resistance of the filament. We assume that this non-linearity is due to the change of filament temperature. Therefore, we can calculate the temperature of the filament using the temperature dependence of a metallic resistance:

$$R = R_0[1+\alpha(T-T_0)] , \tag{3}$$

where R_0 is the estimated resistance of the filament at T_0 (room temperature) which corresponds to the beginning part of RESET plot and α is the resistance temperature coefficient obtained from Figure 10. The resistance in each region of the RESET plot can be estimated by $\partial I/\partial V = 1/R$. Assuming that the filament diameter does not change from room temperature to the highest temperature before rupturing, we calculated the temperature in different regions of the RESET plots for a filament with length of 5 μm and average diameter of 73.2±14.7 nm.

Figure 17 shows the measured I-V curve during the reset process, and the calculated average temperatures of 5 different RESET plots with their standard deviations. These results are consistent with Joule heating occurring during the RESET process. The average temperature before rupturing the filament is calculated to be 798±55 K which can result in melting, sintering or thermal oxidation of cupper nanofilament.[109, 110] Although 798 K is well below the 1356 K melting temperature of bulk Cu, it is reasonable that nanoscale Cu would melt at a lower temperature. Also, if sintering of the material were to occur, a gap could form in the metal filament due to shrinkage during sintering.

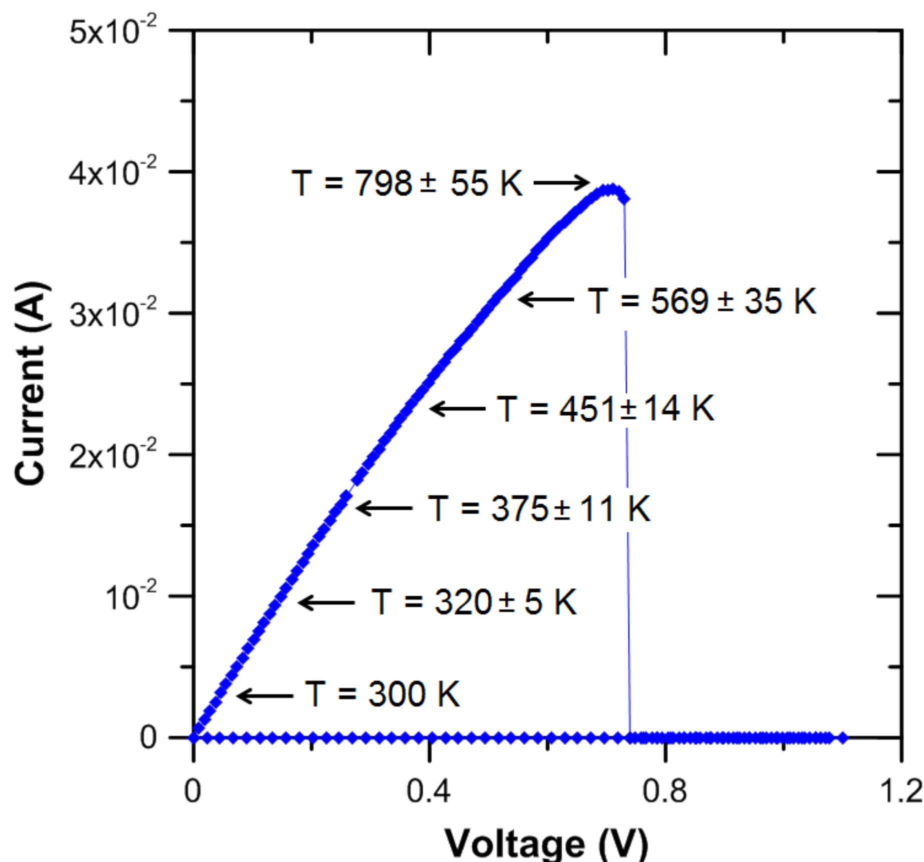

Figure 17. Current-voltage curve of Au/Cu_2O (5 μm thick)/Au-Pd cell during RESET process with calculated temperatures in each region of the plot before rupturing the nanofilament. The reported temperatures are the average of 5 different RESET plots with their standard deviations.

CONCLUSIONS

We studied unipolar resistance switching in electrodeposited cuprous oxide (Cu_2O) thin film. After the FORMING process, Cu_2O shows stable reversible switching with high resistance ratio (R_{HRS}/ R_{LRS}) of about 10^4 for 170 cycles. AC-impedance spectroscopy results and resistance vs. temperature plots suggest formation of a Cu filament in the LRS. Diameter calculations and the obtained value for resistance temperature coefficient in LRS indicate formation of a nanoscale Cu filament during the

SET step. The filament's diameter is a function of compliance current. Increasing the compliance current increases both the filament diameter and the RESET current. At high bias, the as-deposited state shows Poole-Frenkel conduction behavior that is related to point defects in the cuprous oxide. The calculated temperature before rupture of the Cu nanofilament at RESET process suggests the possibility of gap formation due to melting, sintering, or thermal oxidation of the Cu nanofilament due to Joule heating.

AUTHOR INFORMATION

Corresponding Author

*E-mail: jswitzer@mst.edu

ACKNOWLEDGMENTS

This work is supported by the National Science Foundation under grants DMR-1104801 and ECCS-1310425.

II. THE EFFECTIVE PARAMETERS ON RESISTANCE SWITCHING OF ELECTRODEPOSITED CUPROUS OXIDE THIN FILMS

This paper has been prepared for submission to *MATERIALS AND DESIGN*

Sanaz Yazdanparast[1] and Jay A. Switzer[1,2*]

[1]Department of Materials Science and Engineering, Missouri University of Science and Technology, Rolla, Missouri, 65409-1170, United States

[2]Department of Chemistry and Graduate Center for Materials Research, Missouri University of Science and Technology, Rolla, Missouri, 65409-1170, United States

ABSTRACT

In this work, we studied the effect of cuprous oxide microstructure and the top electrode area on resistance switching of electrodeposited cuprous oxide thin films. Different microstructures of cuprous oxide are achieved by changing the applied potential at 50^0 C and by changing the bath temperature in the galvanostatic mode. The applied potential changes both the grain size and orientation of films. Higher negative potentials result in finer grain size with a preferred orientation in the [111] direction. Increasing the bath temperature in galvanostatic electrodeposition increases the grain size of cuprous oxide. All the films in Au/Cu_2O/Au-Pd cell showed unipolar resistance switching behavior after an initial FORMING process. The obtained results show that the microstructure of the deposited films, the orientation of the cuprous oxide grains, and the top electrode area affect the required FORMING voltage. The current level in HRS increases by increasing the top electrode area and decreasing the grain size of cuprous oxide. The independency of current in LRS to the top electrode area suggests the filamentary conduction mechanism in unipolar resistance switching of cuprous oxide thin films.

KEYWORDS

Resistance Switching; Cuprous Oxide Microstructures; Top Electrode Area.

INTRODUCTION

Cuprous oxide is a p-type semiconductor with a direct band gap of 2.0 eV [111] which has recently received much attention due to its potential application in resistance switching random access memory (RRAM) [3, 63]. A RRAM is a nonvolatile memory with a capacitor-like structure composed of an insulating or oxide material between top and bottom metal electrodes [95]. The principle characteristic of the RRAM device is reversible switching of the insulating material between high and low resistance states [59][14].

Typically, a high electric voltage with a compliance current is necessary for most of metal oxides such as cuprous oxide to initiate the reversible resistance switching [26]. This initial process in resistance switching is called FORMING. After FORMING, the material can be switched from a low resistance state (LRS) to a high resistance state (HRS) by a RESET process and from HRS to LRS by a SET process [83]. In spite of the importance of the FORMING step in resistance switching, there is lack of information on the parameters that can affect this process. Generally, a lower FORMING voltage is favorable to have less power consumption and to avoid fatal damage during practical application [39, 112].

Based on the current-voltage (I-V) characteristics, resistance switching can be classified to two groups; unipolar and bipolar switching [80]. In unipolar switching, the required voltages in SET and RESET steps are of the same polarity with different magnitude, while in bipolar switching they are of opposite polarity [34]. These different switching behaviors are dependent on the materials used in RRAM; including the intermediate oxide layer and the electrodes [32, 42].

Although different models have been proposed to clarify the resistance switching mechanism, the origin of resistance switching is still in controversy. Generally, resistance switching mechanism can be categorized according to the conducting path in the LRS; a filamentary conduction path and an interface-type conduction path [6]. In the filamentary conduction path, the formation and rupture of conductive filaments result in resistance switching of oxide materials. In interface-type conducting path, the resistance switching takes place over the entire area of interface between the metal electrode and oxide material [3].

In this work, we have studied the effect of cuprous oxide microstructure and top electrode area on its resistance switching characteristics. To understand the resistance switching mechanism, we have studied the role of top electrode area on the current levels in both LRS and HRS. From the independency of current in LRS to the size of top electrode, we infer formation of a conductive filament as the origin of unipolar resistance switching in Au/Cu_2O/Au-Pd cell.

EXPERIMENTAL PROCEDURE

Cuprous oxide thin films with a thickness of about 3.8 μm were electrodeposited by cathodic reduction of Cu(II) tartrate solution [90] on gold coated glass substrates at different conditions. To obtain different microstructure of cuprous oxide, both potentiostatic and galvanostatic electrodeposition were performed. For all of the electrodepositions, saturated silver chloride (Ag/AgCl) reference electrode was used. In the potentiostatic mode, the electrodeposition was performed at different potentials in the range of -0.394 to -0.283 V at 50° C. In the galvanostatic mode, different microstructures

were achieved at a cathodic current density of 1 mA/cm^2 at different temperature in the range of 25° C -50° C. The structure and phase composition of electrodeposited films were studied by a high resolution Philips X-Pert MRD X-ray diffractometer (XRD) using Cu Kα radiation. The surface and cross section morphologies were observed using a scanning electron microscope (SEM). To measure the resistance switching properties of cuprous oxide thin films, Au-Pd top electrodes with different area of 7.8×10^3 μm^2, 5.4×10^4 μm^2, and 11×10^5 μm^2 were sputtered on the films using a shadow mask. A Sharp Au spring pin contact was used for electrical connection to the top electrodes. Resistance switching measurements were performed using a Keithley 2400 current source at room condition.

RESULTS

Figure 1 shows X-ray diffraction (XRD) patterns of electrodeposited thin films at different potentials. Pure cuprous oxide films are obtained at all the applied potentials. At low negative potentials of -0.283 and -0.294 V cuprous oxide is not oriented while a highly [111]-oriented cuprous oxide is obtained at high negative potential of -0.394 V. Figure 2 shows the cross section images of cuprous oxide thin films electrodeposited at -0.394 and -0.283 V. Electrodeposited films at negative potential of -0.394 V shows oriented grains along [111] direction with columnar structure while random orientation of films is observed at applied potential of -0.283 V. The surface SEM images of the electrodeposited samples at different potentials are shown in Figure 3. Decreasing the applied negative potential results in increasing the grain size of cuprous oxide thin films.

This increase of grain size is presumably due to the lower nucleation density at the more positive potential [91, 113].

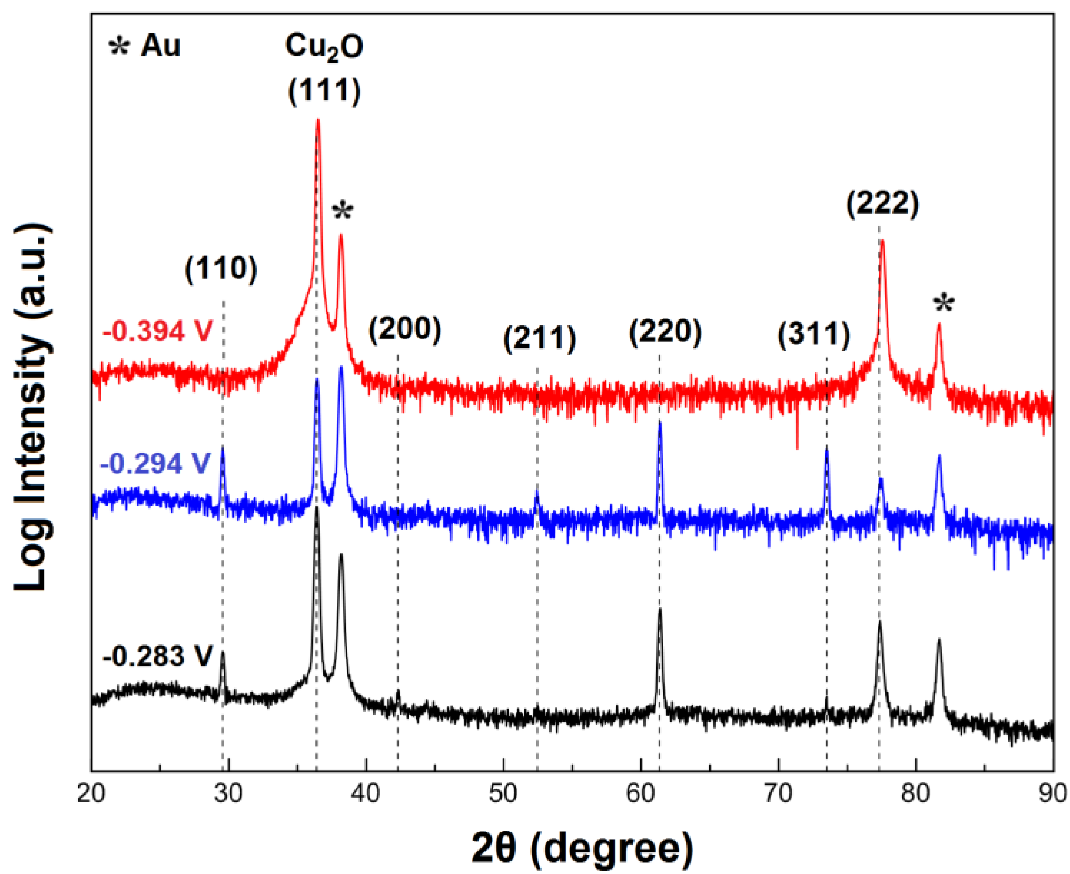

Figure 1. XRD results of electrodeposited cuprous oxide films at a constant temperature of 50^0 C and potentials of -0.394, -0.294, and -0.283 V.

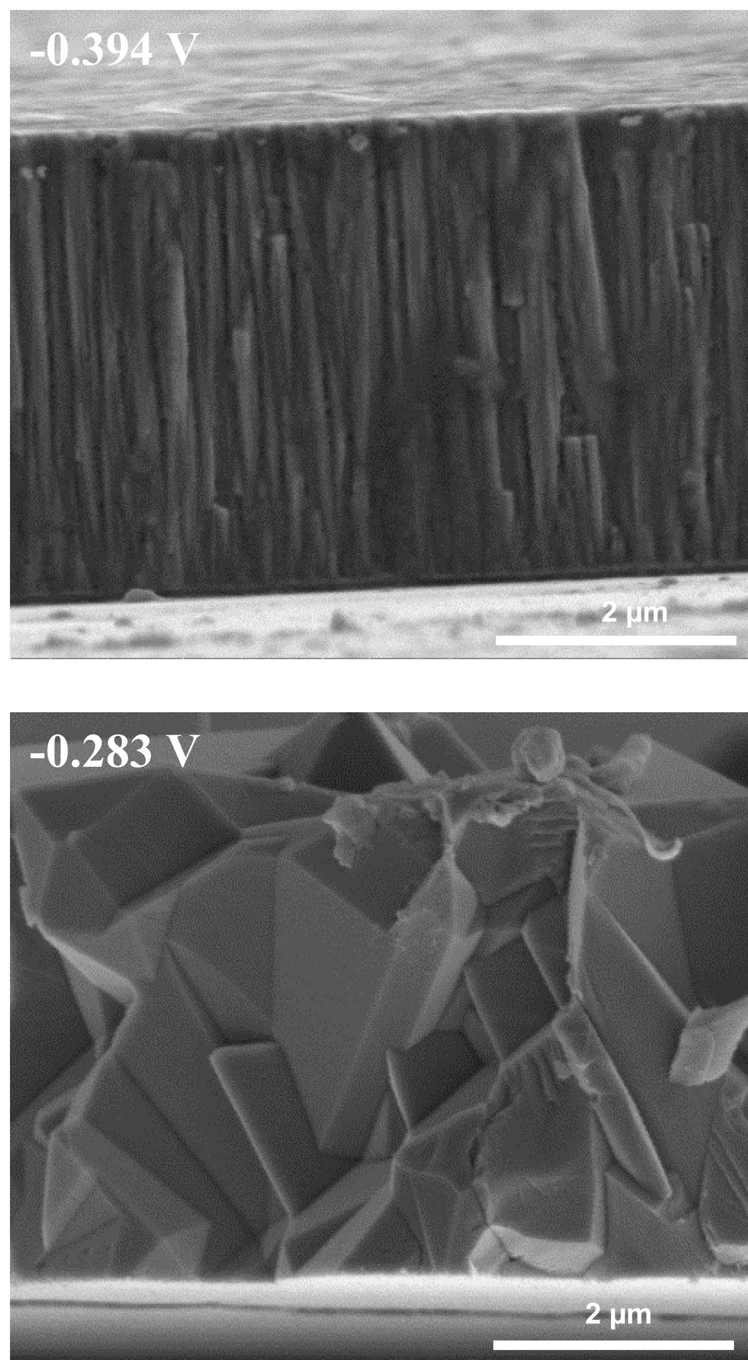

Figure 2. Cross-sectional SEM images of electrodeposited films at -0.394 V (top) and -0.283 V (bottom).

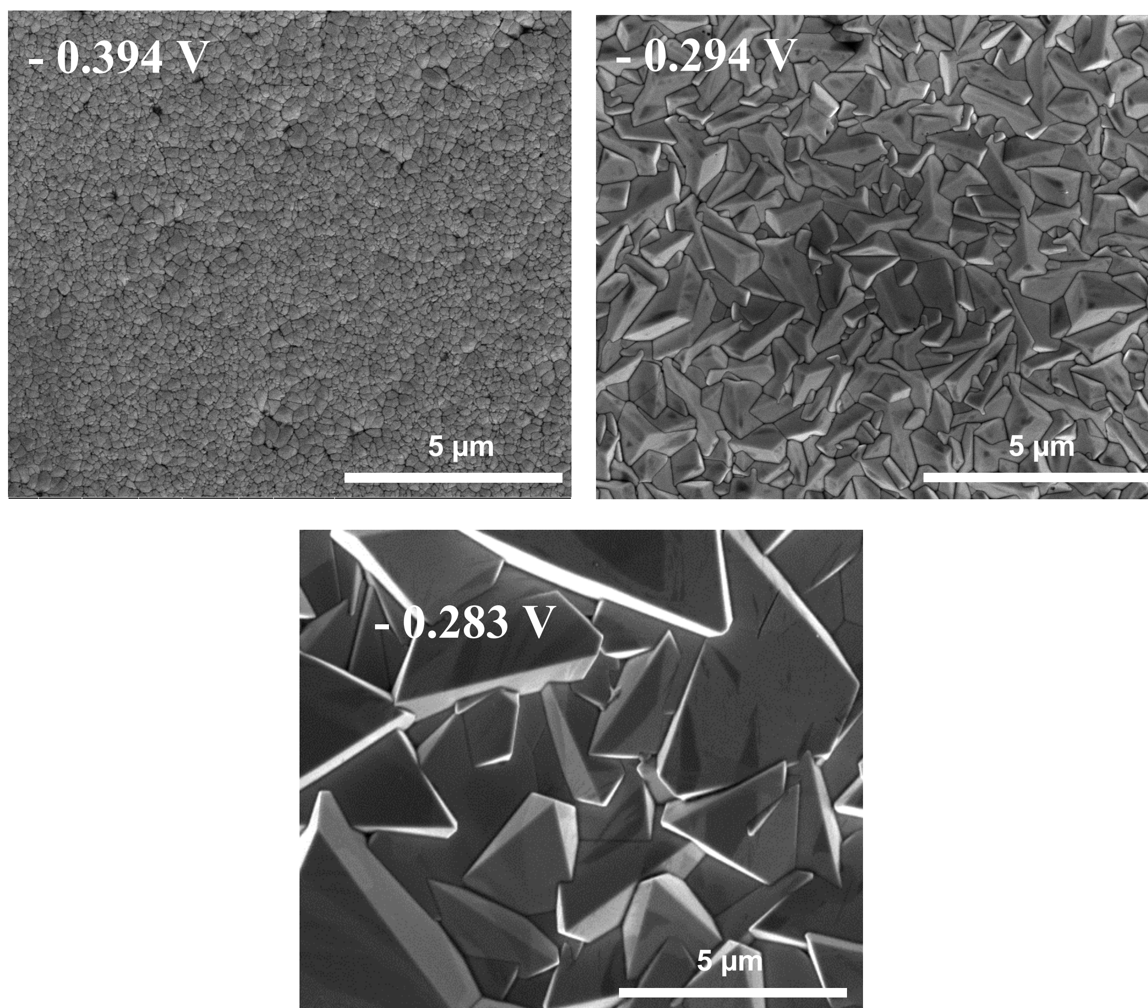

Figure 3. Plan view SEM images of cuprous oxide grains electrodeposited at different potentials.

Figure 4 shows the XRD results of cuprous oxide films electrodeposited at constant current density of $1mA/cm^2$ and different temperatures in the range of 25° C to 50° C. All the cuprous oxide films that are electrodeposited at a constant current density of 1 mA/cm^2 are oriented along the [111] direction. Figure 5 shows the cross sectional SEM images of electrodeposited samples at temperatures of 25 ^{o} C and 40 ^{o} C. The columnar structure of grains with preferred orientation along [111] direction is observed from the cross sectional images. Figure 6 shows the surface morphology of cuprous oxide

films at different electrodeposition temperature. The cuprous oxide grain size increases at higher bath temperature, which can be due to the lower over-potential in electrodeposition at higher bath temperature [113].

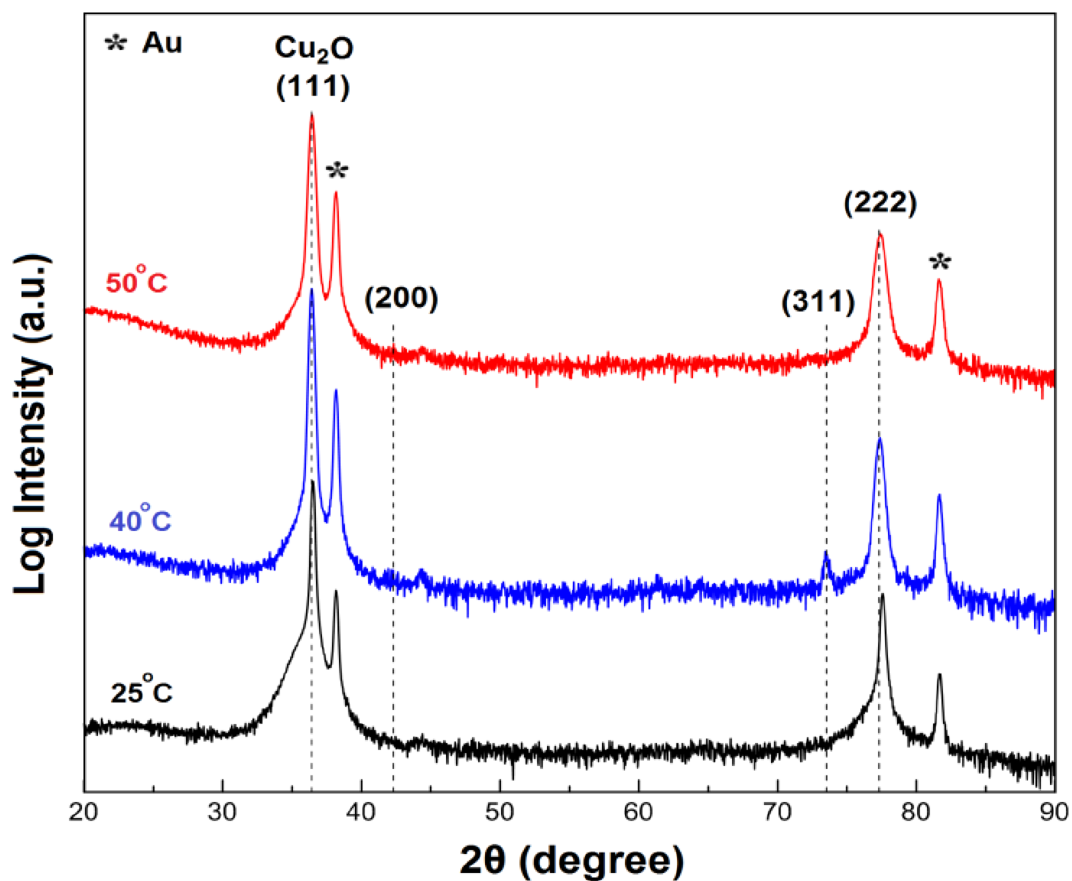

Figure 4. XRD results of electrodeposited cuprous oxide films at constant cathodic current density of 1 mA/cm^2 and different temperatures.

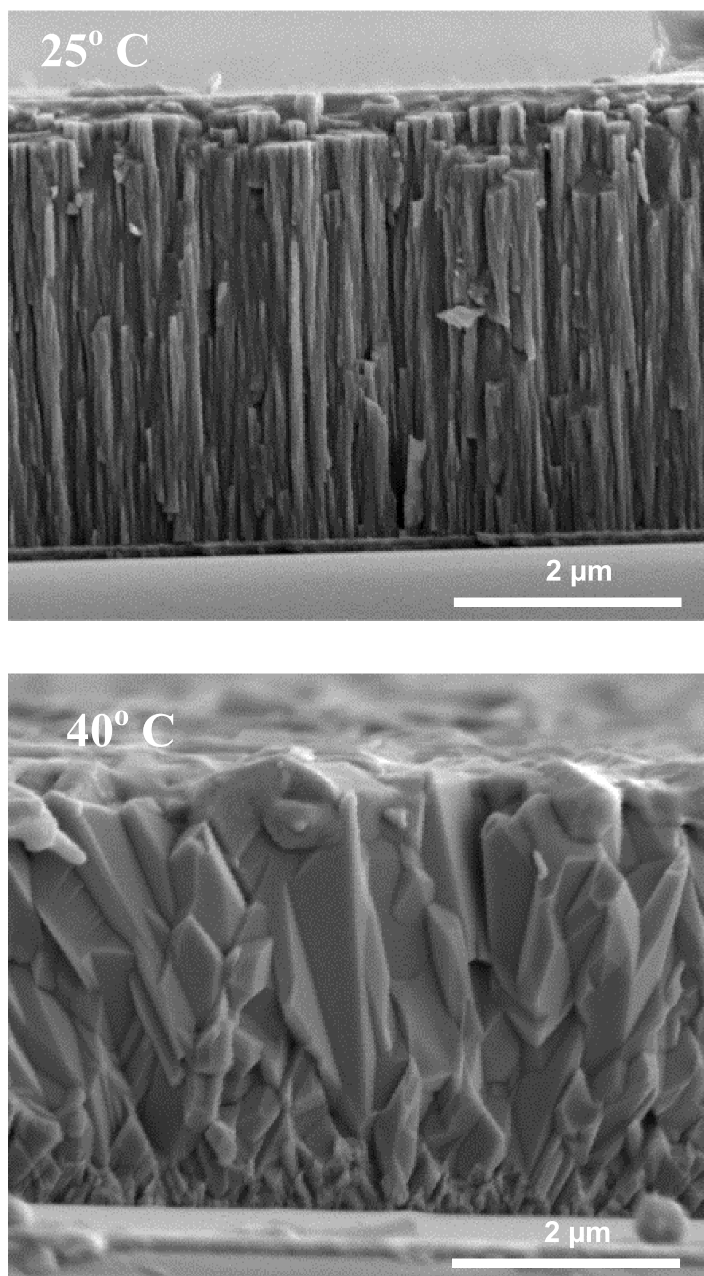

Figure 5. Cross-sectional SEM images of electrodeposited films at 25° and 40 ° C.

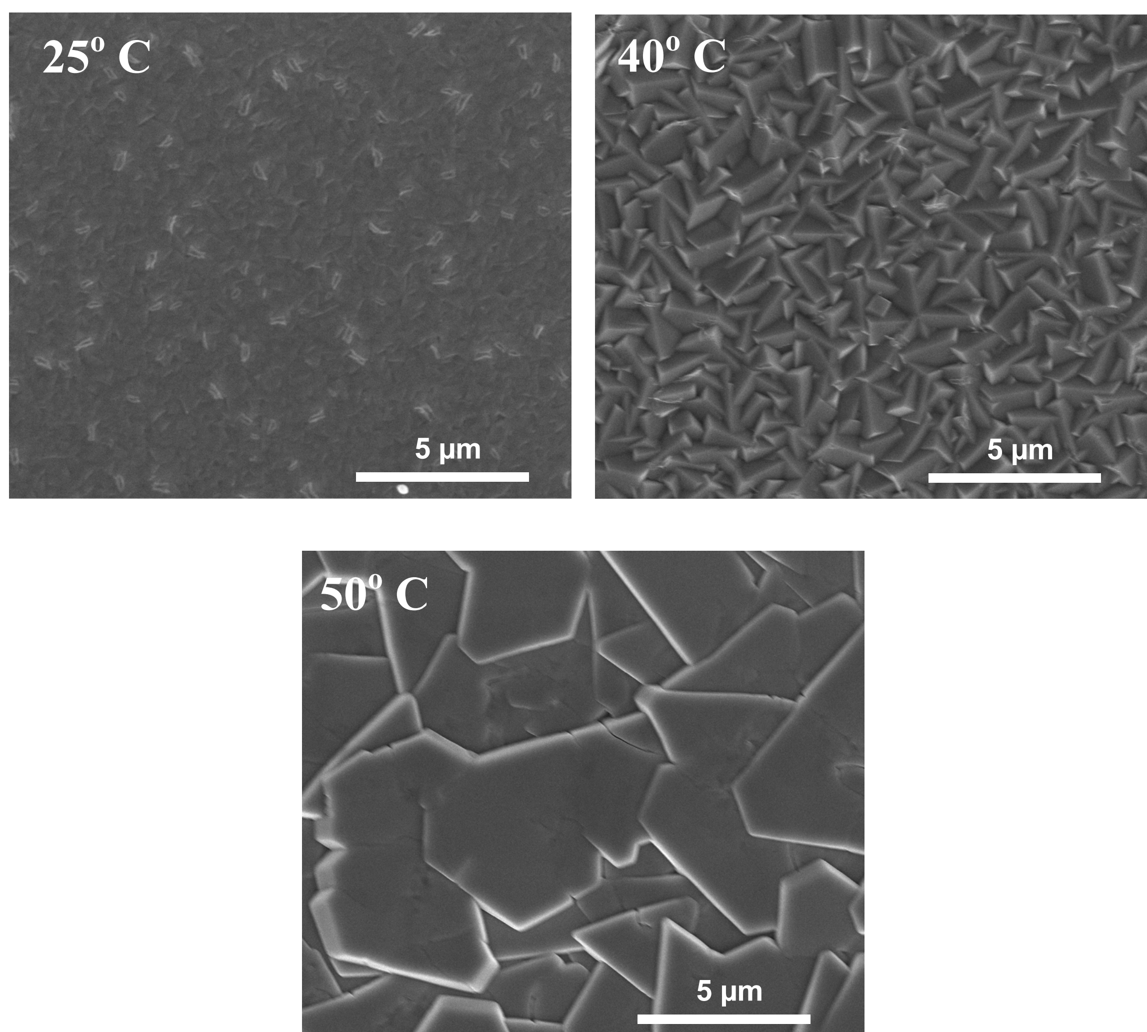

Figure. 6. Plan view SEM images of cuprous oxide grains electrodeposited at different temperatures.

To study the resistance switching of cuprous oxide films, we applied an initial FORMING voltage with compliance current of 5 mA using a top contact area of 7.8×10^3 μm^2. All the films showed unipolar resistance switching. Figure 7 shows the required FORMING voltages for the cuprous oxide thin films that are electrodeposited at different potentials. The FORMING voltage increases as the electrodeposition potential is decreased. This increase of voltage can be due to bigger grain size and/or random orientation of cuprous oxide grains [28].

To clarify the effects of grain size and orientation of cuprous oxide grains on the FORMING voltage, we studied the required FORMING voltages of different microstructures of cuprous oxide with [111]-oriented and columnar structure. Figure 8 shows that increasing the grain size of [111]-oriented cuprous oxide films also results in higher FORMING voltage. Comparing the results of Figures 7 and 8 shows that the required FORMING voltage for the cuprous oxide with average grain size of 3.2 μm and random orientation is higher than cuprous oxide with average grain size of 4.1 μm and highly [111]-oriented grains. If we only consider the effect of microstructure on FORMING voltage, the FORMING voltage should be higher for bigger grain size of cuprous oxide. Therefore, it can be concluded that both microstructure and orientation of cuprous oxide grains affect the FORMING voltage. Increasing the grain size reduces the amount of grain boundary densities which can result in less diffusion path for formation of conductive filaments and/or less defects and higher FORMING voltage. On the other hand, oriented grains and columnar structure of cuprous oxide can form straight filaments along grain boundaries which require lower FORMING voltage [28].

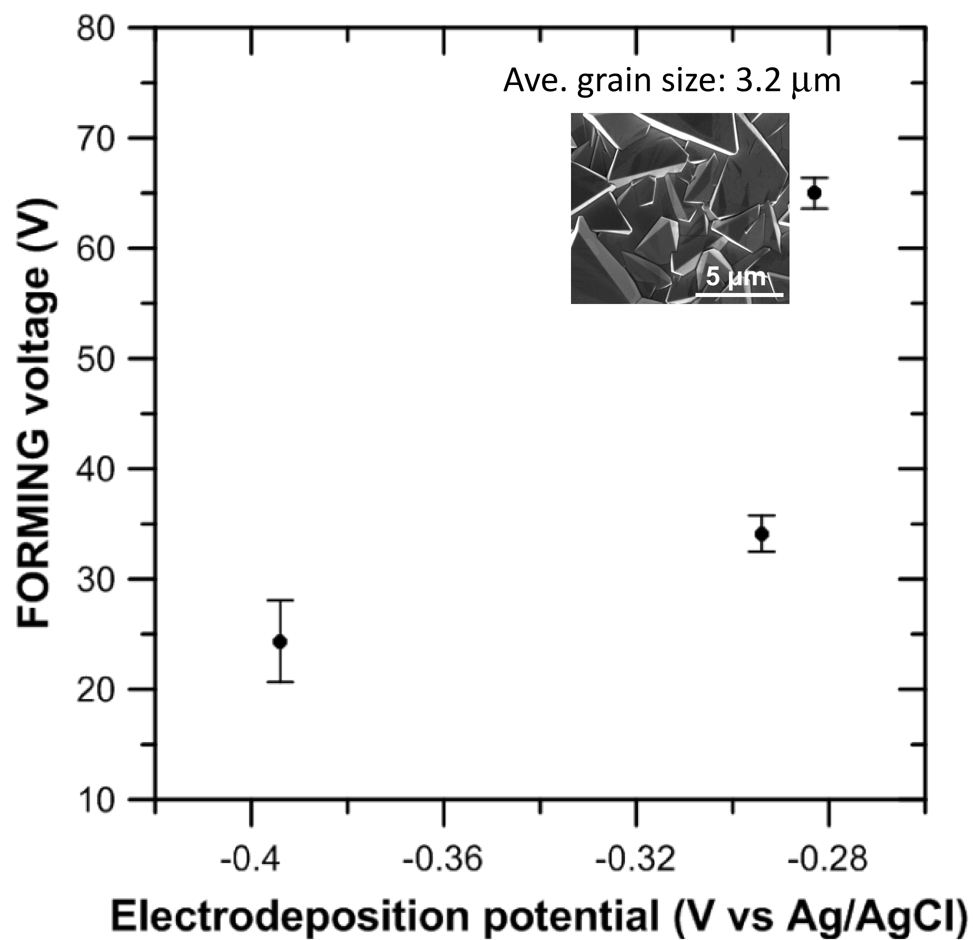

Figure 7. The required FORMING voltage for the cuprous oxide films electrodeposited at different potentials. The solid points show the average value of 5 different contacts with their standard deviations.

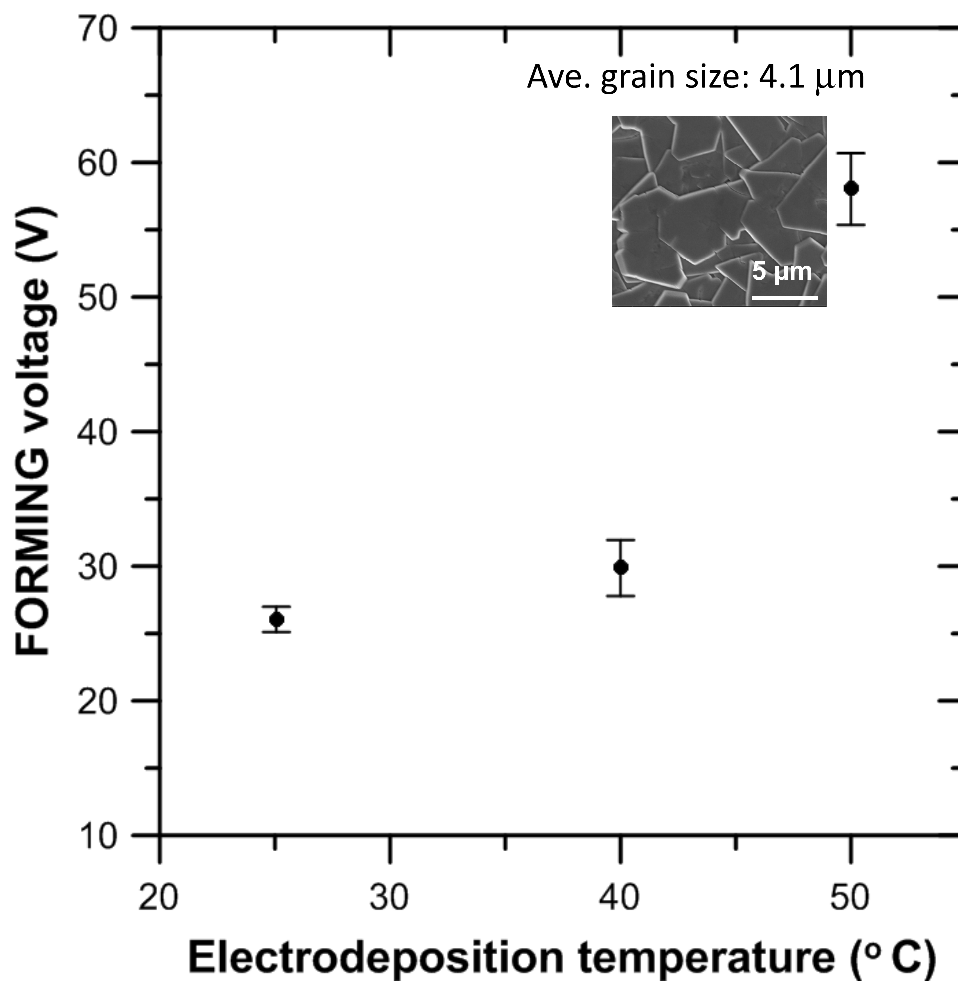

Figure 8. The required FORMING voltage for the cuprous oxide films electrodeposited at galvanostatic mode and different temperatures. The solid points show the average value of 5 different contacts with their standard deviations.

Figure 9 shows V_{SET} and V_{RESET} as a function of cuprous oxide grain size. The SET voltage increases with increasing the grain size, while the RESET voltage is independent of cuprous oxide grain size. We also measured the current level in each state of resistance switching at reading voltage of 0.025 V (Figure 10). There is no change in the current level of LRS when the microstructure of cuprous oxide changes, but the current level of HRS decreases by increasing the grain size. The higher amount of HRS current in finer grain size of cuprous oxide can be due to the reduction of barrier to electron tunneling in grain boundaries, and/or higher concentration of point defects at the grain boundaries [114, 115].

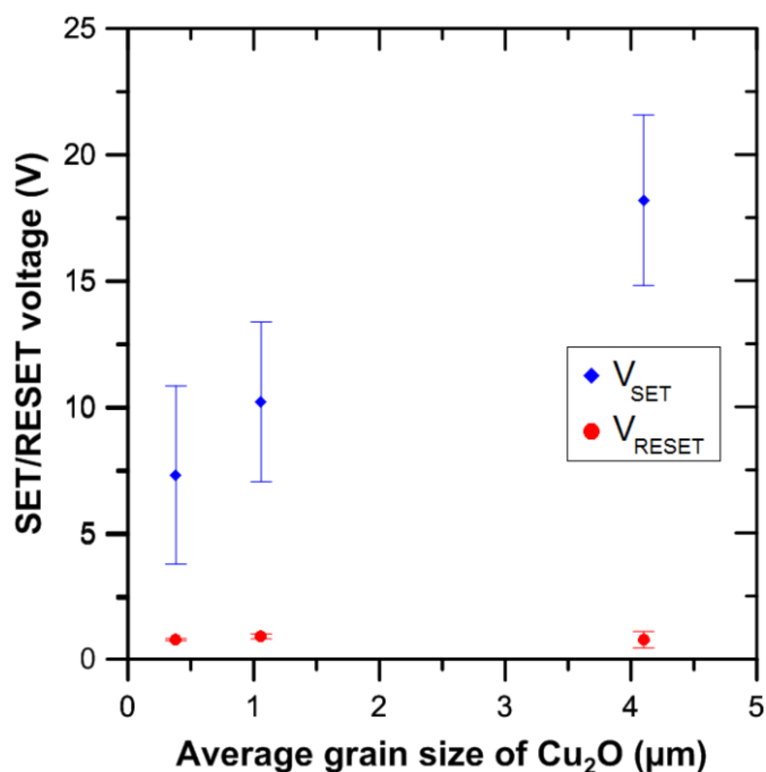

Figure 9. SET and RESET voltages as a function of average grain size of cuprous oxide.

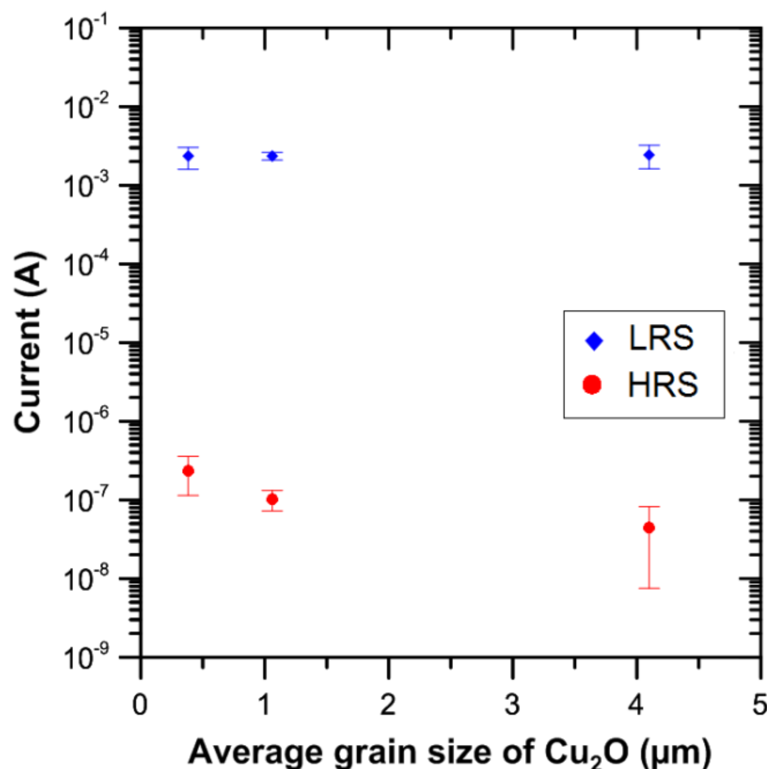

Figure 10. HRS (red circles) and LRS (blue diamonds) current levels vs. average grain size of cuprous oxide. The current was measured at reading voltage of 0.025 V. The solid points show the average values of 5 different contact points with their standard deviations.

To elucidate the resistance switching mechanism, we studied the effect of top electrode area on current levels of LRS and HRS for the sample electrodeposited at cathodic current density of 1 mA/cm^2 and 40^0 C. To switch the as-deposited cuprous oxide thin film to the LRS, a compliance current of 60 mA was used in FORMING process. We observed that the top electrode area affects the required FORMING voltage. Figure 11 shows that FORMING voltage increases by decreasing the top electrode area which is due to increasing the resistance of the cell by decreasing the top electrode area. The measured resistance values from impedance spectroscopy are shown in Table I. After FORMING process, we applied a low voltage with no compliance current to switch the

material from LRS to HRS. Figure 12 shows the current measurements of different states at reading voltage of 0.025 V. The results show that the current of LRS is independent of the contact diameter, demonstrating the current flow through filamentary paths in LRS. The current in HRS increases by increasing the electrode area showing that the current flows homogenously over the entire electrode area.

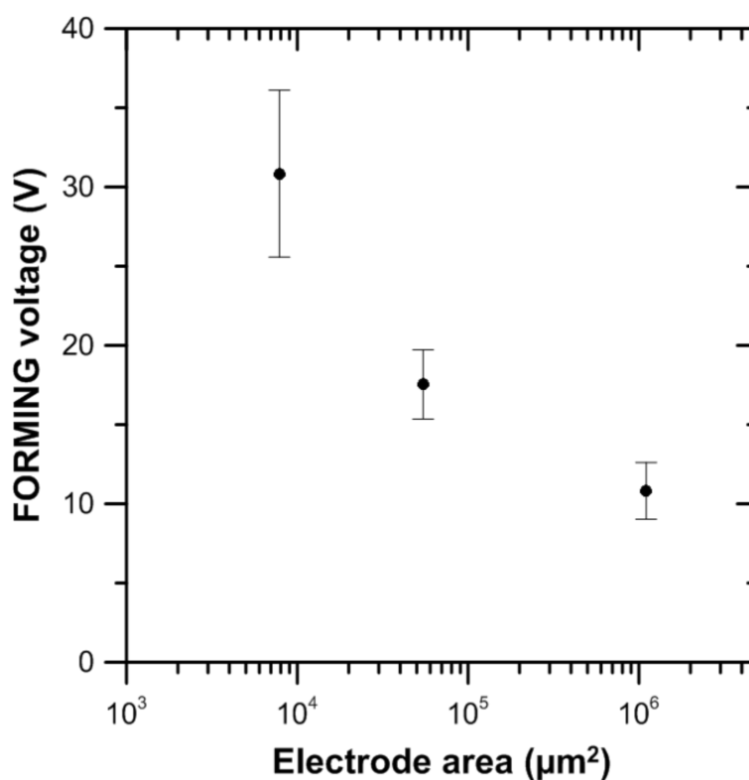

Figure 11. FORMING voltage vs. top electrode area. The solid points show the average values of 5 different contact points with their standard deviations.

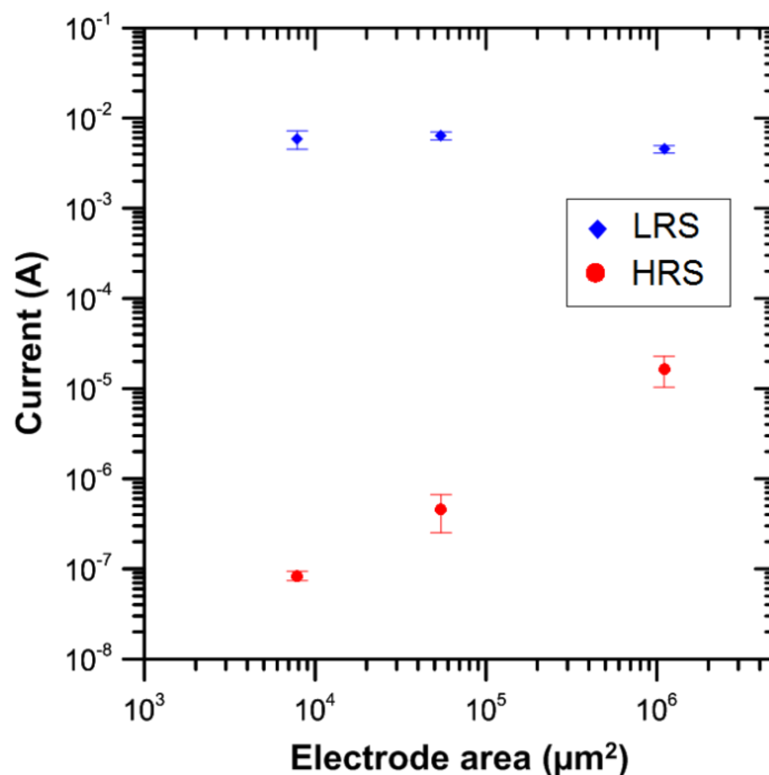

Figure. 12. Current of LRS (blue diamonds) and HRS (red circles) as a function of top electrode area. The currents were measured at reading voltage of 0.025 V. The solid points show the average values of 5 different contact points with their standard deviations.

Table 1. The measured resistance from impedance spectroscopy for Au/Cu_2O/Au-Pd cell with three different top electrode areas.

Top electrode area	7.8×10^3 µm^2	5.4×10^4 µm^2	11×10^5 µm^2
R (Ω)	212290	43378.0	1093.00

CONCLUSIONS

In conclusion, we obtained different microstructure of cuprous oxide thin films by electrodeposition in both potentiostatic and galvanostatic modes. Applying different negative potentials changes both the grain size and orientation of cuprous oxide thin films. Finer grain size with a preferred orientation in [111] direction is achieved at a large

negative potential of -0.396 V. Bath temperature in galvanostatic electrodeposition has a strong effect on grain size of cuprous oxide. The cuprous oxide films in Au/Cu_2O/Au-Pd cell show unipolar resistance switching with an initial FORMING process. FORMING voltage increases with increasing the grain size of cuprous oxide and with decreasing the top electrode area. The current level in HRS decreases by increasing the grain size of cuprous oxide and by decreasing the top electrode area. The obtained results in this study support the filamentary conduction mechanism in unipolar resistance switching of cuprous oxide thin films.

ACKNOWLEDGMENTS

This work is supported by National Science Foundation under grants DMR-1104801 and ECCS-1310425.

PAPER

III. RESISTANCE SWITCHING OF ELECTRODEPOSITED Cu_2O NANOWIRES

This paper has been prepared for submission to *APPLIED PHYSICS LETTERS*

Sanaz Yazdanparast,[1] Jakub A. Koza,[2] and Jay A. Switzer[1,2*]

[1]Department of Materials Science and Engineering, Missouri University of Science and Technology, Rolla, Missouri, 65409-1170, United States

[2]Department of Chemistry and Graduate Center for Materials Research, Missouri University of Science and Technology, Rolla, Missouri, 65409-1170, United States

ABSTRACT

In this work, we studied the resistance switching of Cu_2O nanowires in an Au-Pt/Cu_2O/Au-Pt cell. Cu_2O nanowires are electrodeposited at room temperature. After an initial FORMING process under an electric field of 3×10^6 V/m, A Cu_2O nanowire is switched to the LRS. After FORMING process physical damages are observed in the cell, which may be caused by Joule heating and gas evolution.

KEYWORDS

Cu_2O nanowires; Resistance Switching; FORMING; Joule heating.

INTRODUCTION

Due to the scalability problem of the current Flash memory, semiconductor industries are seeking scalable replacements [7, 78, 116, 117]. Among several types of promising candidates [30, 40, 51, 118], resistance switching random access memory (RRAM) which is based on reversible switching of an insulating or oxide materials has attracted great attention for nonvolatile memory device applications [27, 98, 119]. RRAM has a simple cell structure composed of an oxide material sandwiched between two metal electrodes [23, 37]. Resistance switching can be achieved by applying a voltage bias on one metal electrode while the other metal electrode is grounded [10, 120]. The RRAM operation can be divided to three main steps; FORMING, RESET, and SET [3, 31, 62]. In most of RRAM cells, a FORMING process is necessary to initiate the reversible resistance switching in oxide materials [4]. One can perform the FORMING process by applying a voltage with a compliance current to the cell resulting in switching the material to the low resistance state (LRS) [26, 47]. After this initial process, the material can be switched to the high resistance state (HRS) by the RESET process and then switched back to the LRS by a SET process [29, 59]. Up to now, most of studies have focused on resistance switching of oxide thin films[17, 50, 88, 121] and few studies have investigated the switching behavior of oxide nanowires [16, 122]. Fabricating a resistance switching cell structure composed of oxide nanowire allows us to investigate the scaling potential of RRAM cell. In this work, we obtained Cu_2O nanowires by electrodeposition at room temperature and fabricated an RRAM cell structure using an electron beam to study the resistance switching behavior of metal/ Cu_2O nanowire/metal cell.

EXPERIMENTAL PROCEDURE

Cu_2O nanowires were electrodeposited using a polycarbonate membrane with open pores of 200 nm diameter. Figure 1 shows schematic of growing Cu_2O nanowires. One side of membrane was sputtered by a 100 nm thick layer of gold. On the same side of membrane, Ni was electrodeposited using nickel sulfate solution to cover the open pores of the membrane. Then, on the other side of the membrane, Cu_2O nanowires were grown using Cu (II) tartrate solution; 0.2 M L(+)-tartaric acid, 0.2 M copper (II) sulfate pentahydrate, and 3 M sodium hydroxide [90] at constant potential -0.395 V (vs Ag/AgCl) and room temperature for 1500 s. After electrodeposition of the Cu_2O nanowires, the Ni was removed by grinding and then the nanowires were released by dissolving the polycarbonate membrane in chloroform ($CHCl_3$). Then, acetone was used to float the Cu_2O nanowires. To avoid the agglomeration of nanowires, the acetone suspension was sonicated several times. The as-deposited Cu_2O nanowires were dispersed on Au pattern substrates by dropping acetone containing Cu_2O nanowires. In this way, the acetone is evaporated and the nanowires remain on the substrate. To study the electrical properties of a Cu_2O nanowire and switch it from as-deposited state to the low resistance state (LRS), we chose one of the nanowires located between two parallel lines of Au patterns on glass. Then we used an electron beam and sputtered Pt to connect the Cu_2O nanowire to Au.

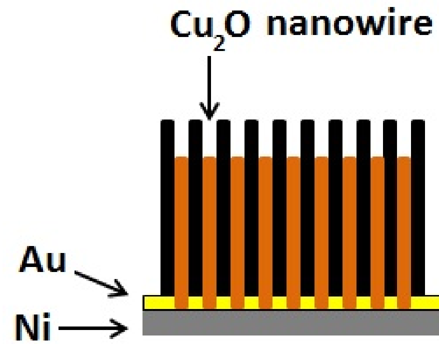

Figure 1. Schematic of growing Cu_2O nanowires.

RESULTS

Figure 2 shows SEM images of the connected Cu_2O nanowire to Au pads using Pt deposition by an electron beam. To switch the nanowire from the as-deposited state to the LRS, we applied a positive voltage to one of the Au electrodes while the other Au electrode was grounded. Figure 3 shows the current-voltage (I-V) curve of the FORMING process. Cu_2O nanowire with length of 2.1 μm switched to the LRS at a forming voltage of 6.3 V which corresponds to an electric field of 3×10^6 V/m. During FORMING, a compliance current of 3 mA was used to avoid the permanent dielectric break-down of Cu_2O nanowire.

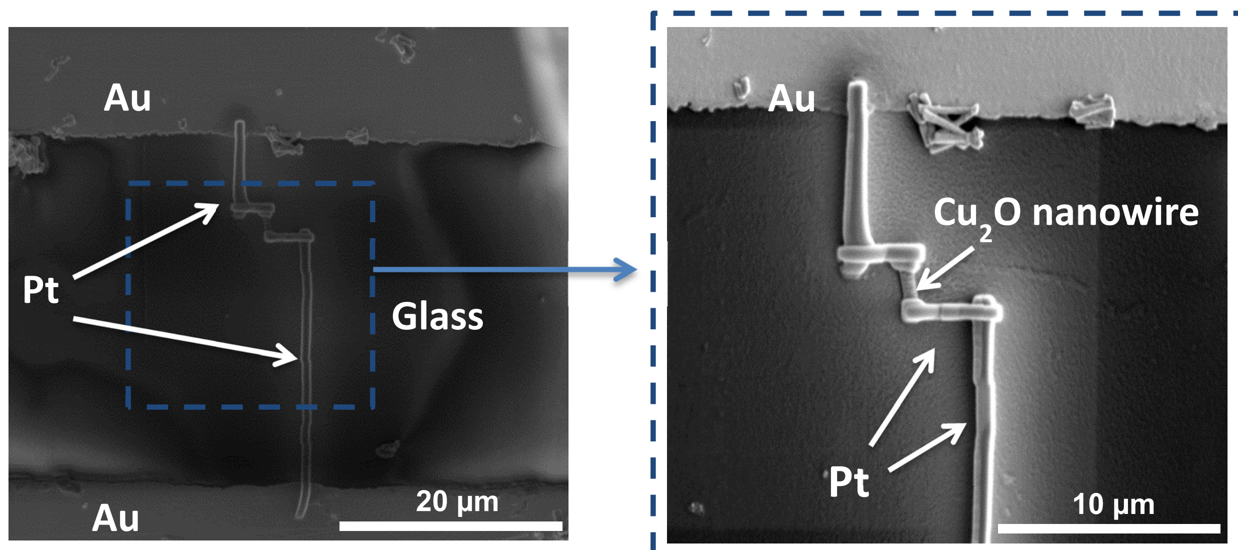

Figure 2. Scanning electron microscopy (SEM) images of a Cu_2O nanowire connected to Au pads using an electron beam and deposition of Pt. The right side image shows a higher magnification of the left side image.

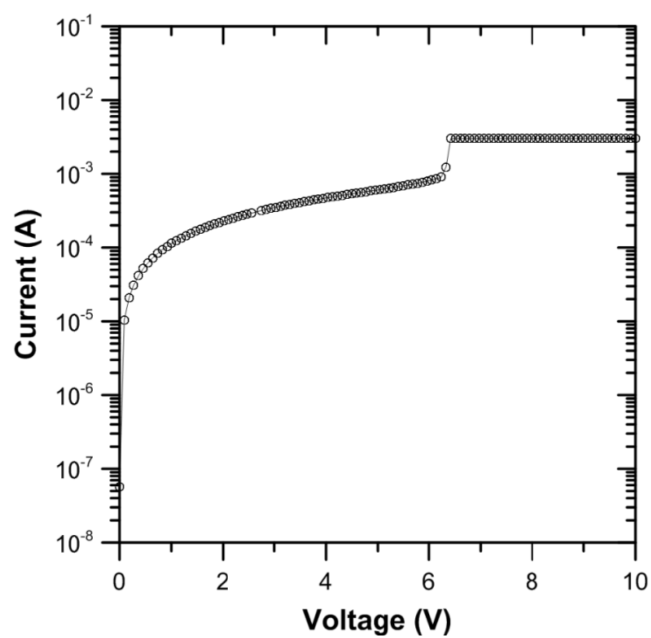

Figure 3. I-V curve of FORMING process showing switching the Cu_2O nanowire to the LRS. During FORMING process the current is limited by the 3 mA compliance current.

Figure 4 shows the SEM image of the Au-Pt/Cu_2O nanowire/Au-Pt cell after FORMING. It is shown that some parts of the Pt and also some materials around the Cu_2O nanowire which are from the deposition of Pt during using electron beam physically damaged during FORMING. This can be due to the Joule heating and oxygen evolution during switching the cell to the LRS.

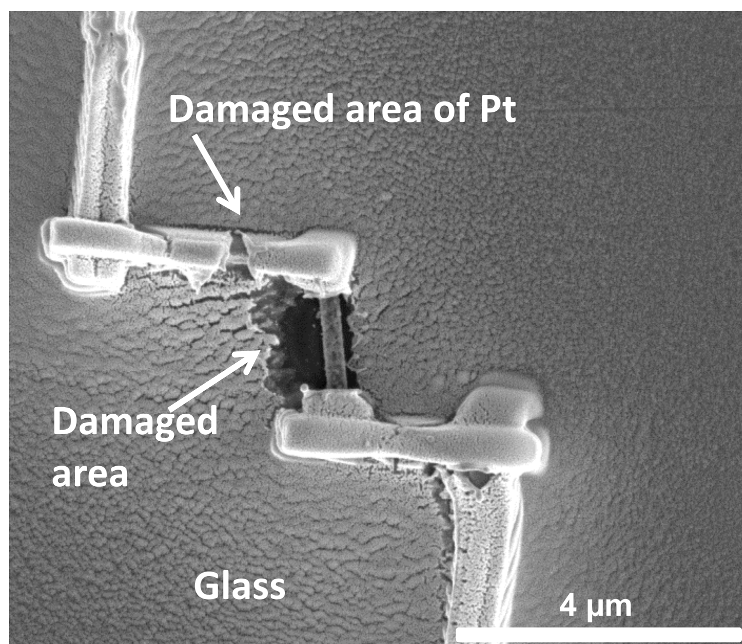

Figure 4. SEM image of Pt/Cu_2O nanowire/Pt cell after FORMING.

CONCLUSIONS

In this work, we electrodeposited Cu_2O nanowires at room temperature and fabricated a RRAM cell structure by an electron beam. After the FORMING process, a Cu_2O nanowire switched to the LRS under an applied electric field of 3×10^6 V/m. After

FORMING process, physical damages to the cell were observed which can be due to Joule heating and oxygen evolution.

ACKNOWLEDGMENTS

This work is supported by National Science Foundation under grants DMR-1104801 and ECCS-1310425.

SECTION

3. CONCLUSIONS AND SUGGESTIONS FOR FUTURE WORKS

The resistance switching behavior of electrodeposited cuprous oxide (Cu_2O) in a cell structure of Au/Cu_2O/Au-Pd was studied. After an initial FORMING process, the fabricated cell showed reversible switching between a LRS (16.6 Ω) and a HRS (0.4×10^6 Ω) by SET and RESET processes. In the LRS, the resistance decreased linearly with decreasing temperature, which was consistent with metallic behavior. The obtained resistance temperature coefficient of material in LRS (1.57×10^{-3} K^{-1}) was similar to that of nanoscale metallic Cu. The switching was attributed to the formation and rupture of Cu nanofilament in Cu_2O due to Joule heating. The filament's diameter was a function of compliance current. Both the filament diameter and the RESET current were increased by increasing the compliance current. At high electric voltage, the as-deposited state showed Poole-Frenkel conduction behavior that was related to point defects in the cuprous oxide.

The results showed that the required FORMING voltage increases with increasing the grain size of cuprous oxide and with decreasing the top electrode area. The current level in LRS was independent to both the grain size of cuprous oxide and the top electrode area suggesting the filamentary conduction mechanism in LRS.

To study the resistance switching mechanism and scalable potential of the cell structure of metal/Cu_2O/metal, Cu_2O nanowires were electrodeposited at room temperature and a RRAM cell structure was fabricated by an electron beam. After the FORMING process, a Cu_2O nanowire was switched to the LRS under an applied electric field of 3×10^6 V/m. After the FORMING process physical damages are observed in the cell, which may be caused by Joule heating and oxygen evolution.

FUTURE WORKS

- A FORMING-free cell (a cell showing resistance switching without an initial FORMING) can result in improving the switching operation and achieving a low power consumption memory. Sufficient defect concentration and nano-thickness of oxide materials may result in a FORMING-free cell. Defect concentration can be controlled by doping different elements to the oxide materials. We suggest studying the effects of different dopants (e.g. Li, Mg, and Zn) on resistance switching of cuprous oxide.
- Low switching cycles (endurance) and non-uniformity of RESET and SET voltages are the critical issues for practical application of RRAM. The switching cycles in RRAM should be more than million cycles to get advantage over current Flash memory. Determining the switching failure can guide us to improve the endurance of RRAM.
- A clear understanding of resistance switching in cuprous oxide is necessary for practical application of this material in RRAM device. We suggest performing the in situ TEM on resistance switching of cuprous oxide to get the critical information of resistance switching.
- Different metal electrodes with lower work function compared to the cuprous oxide show Schottky behavior. We suggest using of this type metal electrodes to make the RRAM cell, and investigate the effect of Schottky contact on resistance switching of cuprous oxide thin films under different bias polarity.

APPENDIX A.

EFFECT OF CUPROUS OXIDE THICKNESS ON FORMING VOLTAGE

We electrodeposited different thickness of cuprous oxide thin films by passage of different amount of charge density at cathodic current density of 1 mA/cm^2 and 60 ^{o}C. To study I-V measurements and study the effect of thickness on FORMING process, we sputtered circular Au-Pd top electrodes with a diameter of 100 μm on the films using a shadow mask. During FORMING process, we observed that the FORMING voltage increases by increasing the cuprous oxide thickness (Figure 1A) which can be due to the increasing the resistance of the film by increasing the thickness[123].

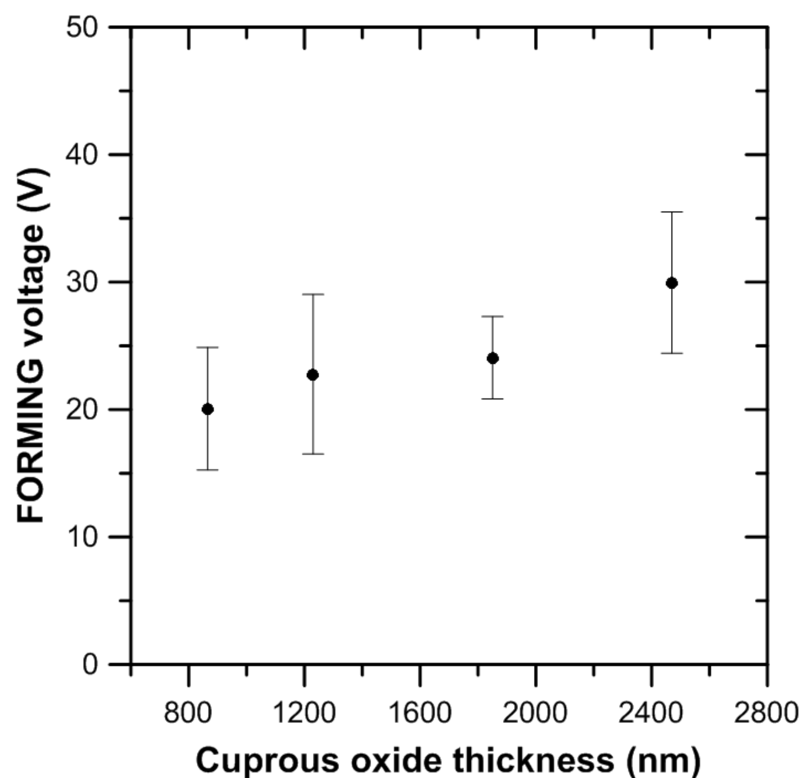

Figure 1A. The required FORMING voltage vs. cuprous oxide thickness.

APPENDIX B.

EFFECT OF TOP ELECTRODE MATERIAL ON FORMING VOLTAGE

We also studied the effect of top electrode material on resistance switching of cuprous oxide thin film. We sputtered two different top electrode materials (Al and Pt) on cuprous oxide films which were electrodeposited at constant cathodic current density of 1 mA/cm^2 and room temperature. The thickness of oxide films was about 3.8µm. In the FORMING process, we observed that the required FORMING voltage for the samples with Al top electrodes is higher than the samples with Pt top electrodes (Figure 1B). From the I-V curves in different polarity, we found that Al forms Schottky barrier contact with cuprous oxide while Pt forms ohmic contact (Figure 2B and Figure 3B). Al has a work function of 4.25 eV which is lower than work function of cuprous oxide (4.84 eV)[124]. When these two materials are connected, the bands bend in cuprous oxide until the chemical potential of semiconductor reaches equilibrium with the Fermi energy of the metal [125, 126]. The deformation of band structure of cuprous oxide forms a potential barrier [124] resulted in higher required FORMING voltage to initiate the resistance switching.

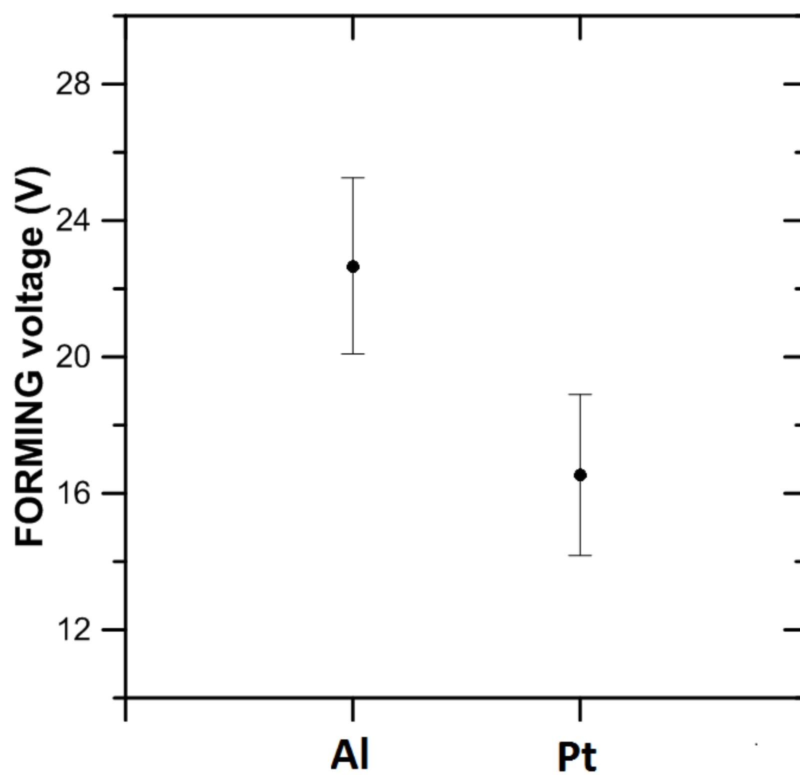

Figure 1B. Effect of top electrode material on the required FORMING voltage in cuprous oxide.

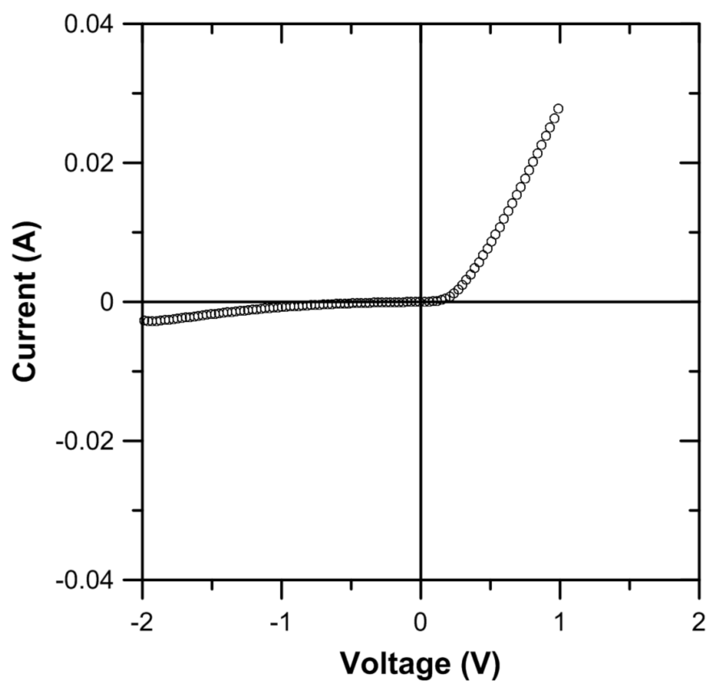

Figure 2B. I-V curve of Al-cuprous oxide contact showing Schottky behavior.

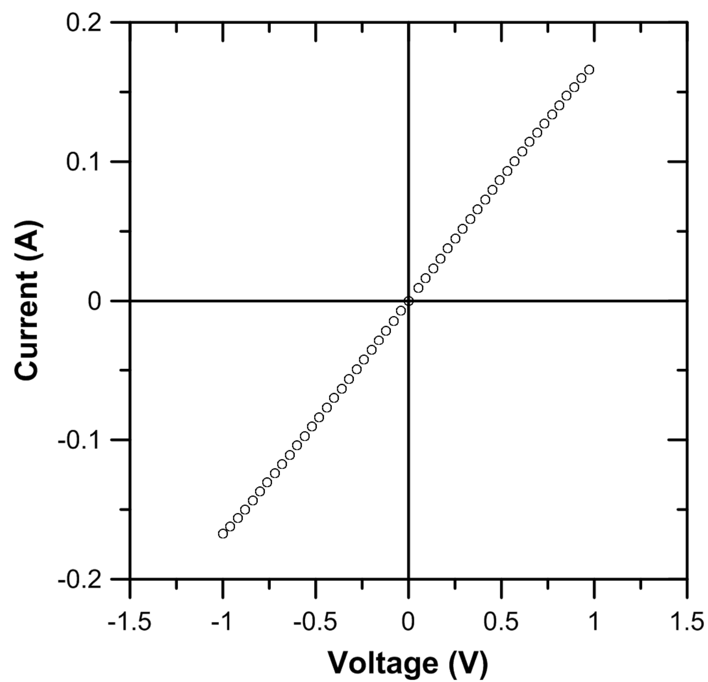

Figure 3B. I-V curve of Pt-cuprous oxide contact showing ohmic behavior.

BIBLIOGRAPHY

1. Liu, C.-Y. and J.-M. Hsu, *Dispersion improvement of unipolar resistive switching Ni/Cu_xO/Cu device by bipolar operation method.* Microelectronic Engineering, 2010. **87**(12): p. 2504-2507.

2. Singh, B., B.R. Mehta, D. Varandani, A.V. Savu, and J. Brugger, *CAFM investigations of filamentary conduction in Cu_2O ReRAM devices fabricated using stencil lithography technique.* Nanotechnology, 2012. **23**(49): p. 495707.

3. Sawa, A., *Resistive switching in transition metal oxides.* MaterialsToday, 2008. **11**(6): p. 28-36.

4. Jeong, D.S., R. Thomas, R.S. Katiyar, J.F. Scott, H. Kohlstedt, A. Petraru, and C.S. Hwang, *Emerging memories: resistive switching mechanisms and current status.* Rep Prog Phys, 2012. **75**(7): p. 076502.

5. Yang, Y.C., F. Pan, Q. Liu, M. Liu, and F. Zeng, *Fully room-temperature-fabricated nonvolatile resistive memory for ultrafast and high-density memory application.* Nano Lett, 2009. **9**(4): p. 1636-43.

6. Pan, F., C. Chen, Z.-s. Wang, Y.-c. Yang, J. Yang, and F. Zeng, *Nonvolatile resistive switching memories-characteristics, mechanisms and challenges.* Progress in Natural Science: Materials International, 2010. **20**: p. 1-15.

7. Shen, Y.-S., B.-S. Chiou, and C.-C. Ho, *Effects of annealing temperature on the resistance switching behavior of $CaCu_3Ti_4O_{12}$ films.* Thin Solid Films, 2008. **517**(3): p. 1209-1213.

8. Lv, H., M. Wang, H. Wan, Y. Song, W. Luo, P. Zhou, T. Tang, Y. Lin, R. Huang, S. Song, J.G. Wu, H.M. Wu, and M.H. Chi, *Endurance enhancement of Cu-oxide based resistive switching memory with Al top electrode.* Applied Physics Letters, 2009. **94**(21): p. 213502.

9. Beck, A., J.G. Bednorz, C. Gerber, C. Rossel, and D. Widmer, *Reproducible switching effect in thin oxide films for memory applications.* Applied Physics Letters, 2000. **77**(1): p. 139-141.

10. Kim, K.M., D.S. Jeong, and C.S. Hwang, *Nanofilamentary resistive switching in binary oxide system; a review on the present status and outlook.* Nanotechnology, 2011. **22**(25): p. 254002.

11. Yoon, M.J., S.B. Lee, H.K. Yoo, S. Sinn, and B.S. Kang, *Dielectric-breakdown-like forming process in the unipolar resistance switching of Ta_2O_{5-x} thin films.* Current Applied Physics, 2012. **12**(3): p. 846-848.

12. Tsubouchi, K., I. Ohkubo, H. Kumigashira, M. Oshima, Y. Matsumoto, K. Itaka, T. Ohnishi, M. Lippmaa, and H. Koinuma, *High-Throughput Characterization of Metal Electrode Performance for Electric-Field-Induced Resistance Switching in Metal/*$Pr_{0.7}Ca_{0.3}MnO_3$*/Metal Structures.* Advanced Materials, 2007. **19**(13): p. 1711-1713.

13. Jiang, X.L., Y.G. Zhao, Y.S. Chen, D. Li, Y.X. Luo, D.Y. Zhao, Z. Sun, J.R. Sun, and H.W. Zhao, *Characteristics of different types of filaments in resistive switching memories investigated by complex impedance spectroscopy.* Applied Physics Letters, 2013. **102**(25): p. 253507.

14. Spiga, S., A. Lamperti, C. Wiemer, M. Perego, E. Cianci, G. Tallarida, H.L. Lu, M. Alia, F.G. Volpe, and M. Fanciulli, *Resistance switching in amorphous and crystalline binary oxides grown by electron beam evaporation and atomic layer deposition.* Microelectronic Engineering, 2008. **85**(12): p. 2414-2419.

15. Park, I.S., J.H. Lee, S. Lee, and J. Ahn, *Resistance switching characteristics of* HfO_2 *film with electrode for resistance change random access memory.* J Nanosci Nanotechnol, 2007. **7**(11): p. 4139-42.

16. Liao, Z.-M., C. Hou, H.-Z. Zhang, D.-S. Wang, and D.-P. Yu, *Evolution of resistive switching over bias duration of single* Ag_2S *nanowires.* Applied Physics Letters, 2010. **96**(20): p. 203109.

17. Choi, B.J., D.S. Jeong, S.K. Kim, C. Rohde, S. Choi, J.H. Oh, H.J. Kim, C.S. Hwang, K. Szot, R. Waser, B. Reichenberg, and S. Tiedke, *Resistive switching mechanism of* TiO_2 *thin films grown by atomic-layer deposition.* Journal of Applied Physics, 2005. **98**(3): p. 033715.

18. Nian, Y.B., J. Strozier, N.J. Wu, X. Chen, and A. Ignatiev, *Evidence for an oxygen diffusion model for the electric pulse induced resistance change effect in transition-metal oxides.* Phys Rev Lett, 2007. **98**(14): p. 146403.

19. Chiu, F.C., P.W. Li, and W.Y. Chang, *Reliability characteristics and conduction mechanisms in resistive switching memory devices using ZnO thin films.* Nanoscale Res Lett, 2012. **7**(1): p. 178.

20. Andam, C.P., G.P. Fournier, and J.P. Gogarten, *Multilevel populations and the evolution of antibiotic resistance through horizontal gene transfer.* FEMS Microbiol Rev, 2011. **35**(5): p. 756-67.

21. Wu, L., X. Li, X. Gao, R. Zheng, F. Zhang, X. Liu, and Q. Wang, *Unipolar resistance switching and abnormal reset behaviors in Pt/CuO/Pt and Cu/CuO/Pt structures.* Solid-State Electronics, 2012. **73**: p. 11-14.

22. Hu, P., X.Y. Li, J.Q. Lu, M. Yang, Q.B. Lv, and S.W. Li, *Oxygen deficiency effect on resistive switching characteristics of copper oxide thin films.* Physics Letters A, 2011. **375**(18): p. 1898-1902.

23. Strukov, D.B. and H. Kohlstedt, *Resistive switching phenomena in thin films: Materials, devices, and applications.* MRS Bulletin, 2012. **37**(02): p. 108-114.

24. Szot, K., W. Speier, G. Bihlmayer, and R. Waser, *Switching the electrical resistance of individual dislocations in single-crystalline* $SrTiO_3$. Nat Mater, 2006. **5**(4): p. 312-20.

25. Yang, Y., W. Lu, Y. Yao, J. Sun, C. Gu, L. Gu, Y. Wang, X. Duan, and R. Yu, *In situ TEM observation of resistance switching in titanate based device.* Sci Rep, 2014. **4**: p. 3890.

26. Lee, S.B., H.K. Yoo, K. Kim, J.S. Lee, Y.S. Kim, S. Sinn, D. Lee, B.S. Kang, B. Kahng, and T.W. Noh, *Forming mechanism of the bipolar resistance switching in double-layer memristive nanodevices.* Nanotechnology, 2012. **23**(31): p. 315202.

27. Yasuhara, R., K. Fujiwara, K. Horiba, H. Kumigashira, M. Kotsugi, M. Oshima, and H. Takagi, *Inhomogeneous chemical states in resistance-switching devices with a planar-type Pt/CuO/Pt structure.* Applied Physics Letters, 2009. **95**(1): p. 012110.

28. Chang, W.-Y., Y.-C. Lai, T.-B. Wu, S.-F. Wang, F. Chen, and M.-J. Tsai, *Unipolar resistive switching characteristics of ZnO thin films for nonvolatile memory applications.* Applied Physics Letters, 2008. **92**(2): p. 022110.

29. Ha, S.D. and S. Ramanathan, *Adaptive oxide electronics: A review.* Journal of Applied Physics, 2011. **110**(7): p. 071101.

30. Huang, J.-J., T.-C. Chang, P.-C. Yang, Y.-T. Chen, H.-C. Tseng, J.-B. Yang, S.M. Sze, A.-K. Chu, and M.-J. Tsai, *Influence of forming process on resistance switching characteristics of* In_2O_3/SiO_2 *bi-layer.* Thin Solid Films, 2013. **528**: p. 31-35.

31. Fujiwara, K., T. Nemoto, M.J. Rozenberg, Y. Nakamura, and H. Takagi, *Resistance Switching and Formation of a Conductive Bridge in Metal/Binary Oxide/Metal Structure for Memory Devices.* Japanese Journal of Applied Physics, 2008. **47**(8): p. 6266-6271.

32. Tang, M.H., B. Jiang, Y.G. Xiao, Z.Q. Zeng, Z.P. Wang, J.C. Li, and J. He, *Top electrode-dependent resistance switching behaviors of ZnO thin films deposited on* $Pt/Ti/SiO_2/Si$ *substrate.* Microelectronic Engineering, 2012. **93**: p. 35-38.

33. Goux, L., J.G. Lisoni, M. Jurczak, D.J. Wouters, L. Courtade, and C. Muller, *Coexistence of the bipolar and unipolar resistive-switching modes in NiO cells made by thermal oxidation of Ni layers.* Journal of Applied Physics, 2010. **107**(2): p. 024512.

34. Kim, K.M., G.H. Kim, S.J. Song, J.Y. Seok, M.H. Lee, J.H. Yoon, and C.S. Hwang, *Electrically configurable electroforming and bipolar resistive switching in Pt/TiO_2/Pt structures.* Nanotechnology, 2010. **21**(30): p. 305203.

35. Kim, C.H., Y.H. Jang, H.J. Hwang, Z.H. Sun, H.B. Moon, and J.H. Cho, *Observation of bistable resistance memory switching in CuO thin films.* Applied Physics Letters, 2009. **94**(10): p. 102107.

36. Herng, T.S., A. Kumar, C.S. Ong, Y.P. Feng, Y.H. Lu, K.Y. Zeng, and J. Ding, *Investigation of the non-volatile resistance change in noncentrosymmetric compounds.* Sci Rep, 2012. **2**: p. 587.

37. Wang, S.-Y., C.-W. Huang, D.-Y. Lee, T.-Y. Tseng, and T.-C. Chang, *Multilevel resistive switching in Ti/Cu_xO/Pt memory devices.* Journal of Applied Physics, 2010. **108**(11): p. 114110.

38. Li, Y., G. Zhao, J. Su, E. Shen, and Y. Ren, *Top electrode effects on resistive switching behavior in CuO thin films.* Applied Physics A, 2011. **104**(4): p. 1069-1073.

39. Li, Y., S. Long, Q. Liu, H. Lü, S. Liu, and M. Liu, *An overview of resistive random access memory devices.* Chinese Science Bulletin, 2011. **56**(28-29): p. 3072-3078.

40. Waser, R. and M. Aono, *Nanoionics-based resistive switching memories.* Nat Mater, 2007. **6**(11): p. 833-40.

41. Lee, M.J., C.B. Lee, D. Lee, S.R. Lee, M. Chang, J.H. Hur, Y.B. Kim, C.J. Kim, D.H. Seo, S. Seo, U.I. Chung, I.K. Yoo, and K. Kim, *A fast, high-endurance and scalable non-volatile memory device made from asymmetric $Ta_2O_{(5-x)}$/$TaO_{(2-x)}$ bilayer structures.* Nat Mater, 2011. **10**(8): p. 625-30.

42. Zhou, Q., Q. Lu, X. Zhang, Y. Song, Y.Y. Lin, and X. Wu, *A study of copper oxide based resistive switching memory by conductive atom force microscope.* Applied Surface Science, 2013. **271**: p. 407-411.

43. Jo, S.H. and W. Lu, *CMOS compatible nanoscale nonvolatile resistance switching memory.* Nano Lett, 2008. **8**(2): p. 392-7.

44. Han, J.-W. and M. Meyyappan, *Copper oxide resistive switching memory for e-textile.* AIP Advances, 2011. **1**(3): p. 032162.

45. Son, J.Y. and Y.H. Shin, *Direct observation of conducting filaments on resistive switching of NiO thin films.* Applied Physics Letters, 2008. **92**(22): p. 222106.

46. Joshua Yang, J., F. Miao, M.D. Pickett, D.A. Ohlberg, D.R. Stewart, C.N. Lau, and R.S. Williams, *The mechanism of electroforming of metal oxide memristive switches.* Nanotechnology, 2009. **20**(21): p. 215201.

47. Lee, S.B., D.H. Kwon, K. Kim, H.K. Yoo, S. Sinn, M. Kim, B. Kahng, and B.S. Kang, *Avoiding fatal damage to the top electrodes when forming unipolar resistance switching in nano-thick material systems.* Journal of Physics D: Applied Physics, 2012. **45**(25): p. 255101.

48. Ahn, S.E., M.J. Lee, Y. Park, B.S. Kang, C.B. Lee, K.H. Kim, S. Seo, D.S. Suh, D.C. Kim, J. Hur, W. Xianyu, G. Stefanovich, H. Yin, I.K. Yoo, J.H. Lee, J.B. Park, I.G. Baek, and B.H. Park, *Write Current Reduction in Transition Metal Oxide Based Resistance Change Memory.* Advanced Materials, 2008. **20**(5): p. 924-928.

49. Xu, N., L. Liu, X. Sun, X. Liu, D. Han, Y. Wang, R. Han, J. Kang, and B. Yu, *Characteristics and mechanism of conduction/set process in TiN/ZnO/Pt resistance switching random-access memories.* Applied Physics Letters, 2008. **92**(23): p. 232112.

50. Huang, C.H., J.S. Huang, C.C. Lai, H.W. Huang, S.J. Lin, and Y.L. Chueh, *Manipulated transformation of filamentary and homogeneous resistive switching on ZnO thin film memristor with controllable multistate.* ACS Appl Mater Interfaces, 2013. **5**(13): p. 6017-23.

51. Wang, J.-C., D.-Y. Jian, Y.-R. Ye, L.-C. Chang, and C.-S. Lai, *Characteristics of gadolinium oxide resistive switching memory with Pt–Al alloy top electrode and post-metallization annealing.* Journal of Physics D: Applied Physics, 2013. **46**(27): p. 275103.

52. Wang, S.-Y., D.-Y. Lee, T.-Y. Tseng, and C.-Y. Lin, *Effects of Ti top electrode thickness on the resistive switching behaviors of rf-sputtered ZrO_2memory films.* Applied Physics Letters, 2009. **95**(11): p. 112904.

53. Lee, M.J., S. Han, S.H. Jeon, B.H. Park, B.S. Kang, S.E. Ahn, K.H. Kim, C.B. Lee, C.J. Kim, I.K. Yoo, D.H. Seo, X.S. Li, J.B. Park, J.H. Lee, and Y. Park, *Electrical manipulation of nanofilaments in transition-metal oxides for resistance-based memory.* Nano Lett, 2009. **9**(4): p. 1476-81.

54. Kim, D.C., S. Seo, S.E. Ahn, D.S. Suh, M.J. Lee, B.H. Park, I.K. Yoo, I.G. Baek, H.J. Kim, E.K. Yim, J.E. Lee, S.O. Park, H.S. Kim, U.I. Chung, J.T. Moon, and B.I. Ryu, *Electrical observations of filamentary conductions for the resistive memory switching in NiO films.* Applied Physics Letters, 2006. **88**(20): p. 202102.

55. Lin, K.-L., T.-H. Hou, J. Shieh, J.-H. Lin, C.-T. Chou, and Y.-J. Lee, *Electrode dependence of filament formation in HfO_2 resistive-switching memory.* Journal of Applied Physics, 2011. **109**(8): p. 084104.

56. Rahaman, S.Z., S. Maikap, T.C. Tien, H.Y. Lee, W.S. Chen, F.T. Chen, M.J. Kao, and M.J. Tsai, *Excellent resistive memory characteristics and switching mechanism using a Ti nanolayer at the Cu/TaO_x interface.* Nanoscale Res Lett, 2012. **7**(1): p. 345.

57. Hong, D.S., Y.S. Chen, Y. Li, H.W. Yang, L.L. Wei, B.G. Shen, and J.R. Sun, *Evolution of conduction channel and its effect on resistance switching for Au-WO_{3-x}-Au devices.* Sci Rep, 2014. **4**: p. 4058.

58. Tulu, B., W.Z. Chang, J.P. Chu, and S.F. Wang, *Forming-free resistive switching characteristics of 15 nm-thick multicomponent oxide.* Applied Physics Letters, 2013. **103**(25): p. -.

59. Kwon, D.H., K.M. Kim, J.H. Jang, J.M. Jeon, M.H. Lee, G.H. Kim, X.S. Li, G.S. Park, B. Lee, S. Han, M. Kim, and C.S. Hwang, *Atomic structure of conducting nanofilaments in TiO_2 resistive switching memory.* Nat Nanotechnol, 2010. **5**(2): p. 148-53.

60. Johnson, S.L., A. Sundararajan, D.P. Hunley, and D.R. Strachan, *Memristive switching of single-component metallic nanowires.* Nanotechnology, 2010. **21**(12): p. 125204.

61. Yang, J.J., M.D. Pickett, X. Li, D.A. Ohlberg, D.R. Stewart, and R.S. Williams, *Memristive switching mechanism for metal/oxide/metal nanodevices.* Nat Nanotechnol, 2008. **3**(7): p. 429-33.

62. Chen, J.Y., C.L. Hsin, C.W. Huang, C.H. Chiu, Y.T. Huang, S.J. Lin, W.W. Wu, and L.J. Chen, *Dynamic evolution of conducting nanofilament in resistive switching memories.* Nano Lett, 2013. **13**(8): p. 3671-7.

63. Chu, D., A. Younis, T. Teck Tan, and S. Li, *Resistive switching behaviors in electrodeposited $BaTiOF_4$ nanorod layers.* Solid State Communications, 2013. **156**: p. 38-40.

64. Kim, S.I., J.H. Lee, Y.W. Chang, S.S. Hwang, and K.-H. Yoo, *Reversible resistive switching behaviors in NiO nanowires.* Applied Physics Letters, 2008. **93**(3): p. 033503.

65. Lee, S.R., H.M. Kim, K. Char, J.H. Jang, M. Kim, M.R. Cho, Y.D. Park, R. Jung, D.C. Kim, and S. Seo, *Role of oxygen vacancies formed between top electrodes and epitaxial NiO films in bipolar resistance switching.* Current Applied Physics, 2012. **12**(2): p. 369-372.

66. Strachan, J.P., M.D. Pickett, J.J. Yang, S. Aloni, A.L. David Kilcoyne, G. Medeiros-Ribeiro, and R. Stanley Williams, *Direct identification of the conducting channels in a functioning memristive device.* Adv Mater, 2010. **22**(32): p. 3573-7.

67. Zhu, W., T.P. Chen, Y. Liu, and S. Fung, *Conduction mechanisms at low- and high-resistance states in aluminum/anodic aluminum oxide/aluminum thin film structure.* Journal of Applied Physics, 2012. **112**(6): p. 063706.

68. Choi, J.S., J.S. Kim, I.R. Hwang, S.H. Hong, S.H. Jeon, S.O. Kang, B.H. Park, D.C. Kim, M.J. Lee, and S. Seo, *Different resistance switching behaviors of NiO thin films deposited on Pt and $SrRuO_3$ electrodes.* Applied Physics Letters, 2009. **95**(2): p. 022109.

69. Pabst, G.W., L.W. Martin, Y.-H. Chu, and R. Ramesh, *Leakage mechanisms in BiFeO[sub 3] thin films.* Applied Physics Letters, 2007. **90**(7): p. 072902.

70. Lampert, M., *Simplified Theory of Space-Charge-Limited Currents in an Insulator with Traps.* Physical Review, 1956. **103**(6): p. 1648-1656.

71. Chiu, F.-C., *A Review on Conduction Mechanisms in Dielectric Films.* Advances in Materials Science and Engineering, 2014. **2014**: p. 1-18.

72. Simmons, J., *Poole-Frenkel Effect and Schottky Effect in Metal-Insulator-Metal Systems.* Physical Review, 1967. **155**(3): p. 657-660.

73. Mitrofanov, O., *Poole-Frenkel electron emission from the traps in AlGaN/GaN transistors.* Journal of Applied Physics, 2004. **95**(11): p. 6414.

74. Chiu, F.-C., Z.-H. Lin, C.-W. Chang, C.-C. Wang, K.-F. Chuang, C.-Y. Huang, J.Y.-m. Lee, and H.-L. Hwang, *Electron conduction mechanism and band diagram of sputter-deposited Al/ZrO_2/Si structure.* Journal of Applied Physics, 2005. **97**(3): p. 034506.

75. Cook, E.L., *Model for the Resistive-Conductive Transition in Reversible Resistance-Switching Solids.* Journal of Applied Physics, 1970. **41**(2): p. 551.

76. Severdenko, V.P., V.A. Labunov, E.M. Kosarevitsh, L.V. Kogietov, and V.M. Parkun, *INVESTIGATION OF THE GROWTH PROCESS AND SWITCHING EFFECTS IN ANODIC COPPER OXIDE FILMS.* Thin Solid Films, 1977. **41**: p. 243-246.

77. Zarabi, M.J. and M. Satyam, *Switching in copper oxide.* Journal of Applied Physics, 1974. **45**(2): p. 775.

78. Chen, A., S. Haddad, Y.C. Wu, Z. Lan, T.N. Fang, and S. Kaza, *Switching characteristics of Cu_2O metal-insulator-metal resistive memory.* Applied Physics Letters, 2007. **91**(12): p. 123517.

79. Park, G.-S., X.-S. Li, D.-C. Kim, R.-J. Jung, M.-J. Lee, and S. Seo, *Observation of electric-field induced Ni filament channels in polycrystalline NiO_x film.* Applied Physics Letters, 2007. **91**(22): p. 222103.

80. Park, C., S.H. Jeon, S.C. Chae, S. Han, B.H. Park, S. Seo, and D.-W. Kim, *Role of structural defects in the unipolar resistive switching characteristics of Pt/NiO/Pt structures.* Applied Physics Letters, 2008. **93**(4): p. 042102.

81. Lee, C.B., B.S. Kang, A. Benayad, M.J. Lee, S.E. Ahn, K.H. Kim, G. Stefanovich, Y. Park, and I.K. Yoo, *Effects of metal electrodes on the resistive memory switching property of NiO thin films.* Applied Physics Letters, 2008. **93**(4): p. 042115.

82. Lee, M.-J., S. Han, S.H. Jeon, B.H. Park, B.S. Kang, S.-E. Ahn, K.H. Kim, C.B. Lee, C.J. Kim, I.-K. Yoo, D.H. Seo, X.-S. Li, J.-B. Park, J.-H. Lee, and Y. Park, *Electrical Manipulation of Nanofilaments in Transition-Metal Oxides for Resistance-Based Memory.* Nano Letters, 2009. **9**(4): p. 1476-1481.

83. Kim, K.M., B.J. Choi, Y.C. Shin, S. Choi, and C.S. Hwang, *Anode-interface localized filamentary mechanism in resistive switching of TiO_2 thin films.* Applied Physics Letters, 2007. **91**(1): p. 012907.

84. Zhuge, F., S. Peng, C. He, X. Zhu, X. Chen, Y. Liu, and R.W. Li, *Improvement of resistive switching in Cu/ZnO/Pt sandwiches by weakening the randomicity of the formation/rupture of Cu filaments.* Nanotechnology, 2011. **22**(27): p. 275204.

85. Younis, A., D. Chu, and S. Li, *Bi-stable resistive switching characteristics in Ti-doped ZnO thin films.* Nanoscale Res Lett, 2013. **8**(1): p. 154.

86. Sim, H., D. Choi, D. Lee, M. Hasan, C.B. Samantaray, and H. Hwang, *Reproducible resistance switching characteristics of pulsed laserdeposited polycrystalline Nb_2O_5.* Microelectronic Engineering, 2005. **80**: p. 260-263.

87. Lee, D., D.-j. Seong, I. Jo, F. Xiang, R. Dong, S. Oh, and H. Hwang, *Resistance switching of copper doped MoO_x films for nonvolatile memory applications.* Applied Physics Letters, 2007. **90**(12): p. 122104.

88. Kang, S.-O., S. Hong, J. Choi, J.-S. Kim, I. Hwang, I.-S. Byun, K.-S. Yun, and B.H. Park, *Electrochemical growth and resistive switching of flat-surfaced and (111)-oriented Cu_2O films.* Applied Physics Letters, 2009. **95**(9): p. 092108.

89. Maruyama, T., *Copper oxide thin films prepared by chemical vapor deposition from copper dipivaloylmethanate.* Solar Energy Materials and Solar Cells, 1998. **56**(1): p. 85-92.

90. Poizot, P., C.-J. Hung, M.P. Nikiforov, E.W. Bohannan, and J.A. Switzer, *An Electrochemical Method for CuO Thin Film Deposition from Aqueous Solution.* Electrochemical and Solid-State Letters, 2003. **6**(2): p. C21.

91. Zhou, Y.C. and J.A. Switzer, *Galvanostatic electrodeposition and microstructure of copper (I) oxide film.* Material Research Innovations, 1998. **2**(1): p. 22-27.

92. Chen, A., S. Haddad, Y.C. Wu, T.N. Fang, S. Kaza, and Z. Lan, *Erasing characteristics of Cu_2O metal-insulator-metal resistive switching memory.* Applied Physics Letters, 2008. **92**(1): p. 013503.

93. Hong, S., D. Xiao Long, I. Hwang, J.-S. Kim, Y. Chang Park, S.-O. Kang, and B. Ho Park, *Unipolar resistive switching mechanism speculated from irreversible low resistance state of Cu_2O films.* Applied Physics Letters, 2011. **99**(5): p. 052105.

94. Gao, S.-m., H. Wang, J.-w. Xu, C.-l. Yuan, and X.-w. Zhang, *Effect of annealing temperature on resistance switching behavior of $Mg_{0.2}Zn_{0.8}O$ thin films deposited on ITO glass.* Solid-State Electronics, 2012. **76**: p. 40-43.

95. Yoon, J., J. Lee, H. Choi, J.-B. Park, D.-j. Seong, W. Lee, C. Cho, S. Kim, and H. Hwang, *Analysis of copper ion filaments and retention of dual-layered devices for resistance random access memory applications.* Microelectronic Engineering, 2009. **86**(7-9): p. 1929-1932.

96. Yang, L., C. Kuegeler, K. Szot, A. Ruediger, and R. Waser, *The influence of copper top electrodes on the resistive switching effect in TiO_2 thin films studied by conductive atomic force microscopy.* Applied Physics Letters, 2009. **95**(1): p. 013109.

97. Dong, R., D.S. Lee, W.F. Xiang, S.J. Oh, D.J. Seong, S.H. Heo, H.J. Choi, M.J. Kwon, S.N. Seo, M.B. Pyun, M. Hasan, and H. Hwang, *Reproducible hysteresis and resistive switching in metal-Cu_xO-metal heterostructures.* Applied Physics Letters, 2007. **90**(4): p. 042107.

98. Sun, X., G. Li, X.a. Zhang, L. Ding, and W. Zhang, *Coexistence of the bipolar and unipolar resistive switching behaviours in Au/$SrTiO_3$/Pt cells.* Journal of Physics D: Applied Physics, 2011. **44**(12): p. 125404.

99. Celano, U., Y. Yin Chen, D.J. Wouters, G. Groeseneken, M. Jurczak, and W. Vandervorst, *Filament observation in metal-oxide resistive switching devices.* Applied Physics Letters, 2013. **102**(12): p. 121602.

100. Koza, J.A., E.W. Bohannan, and J.A. Switzer, *Superconducting filaments formed during nonvolatile resistance switching in electrodeposited δ-Bi_2O_3.* ACS Nano, 2013. **7**(11): p. 9940-6.

101. Tang, Y., Z. Chen, Z. Jia, L. Zhang, and J. Li, *Electrodeposition and characterization of nanocrystalline cuprous oxide thin films on TiO_2 films.* Materials Letters, 2005. **59**(4): p. 434-438.

102. Switzer, J.A., C.-J. Hung, L.-Y. Huang, E.R. Switzer, D.R. Kammler, T.D. Golden, and E.W. Bohannan, *Electrochemical Self-Assembly of Copper/Cuprous Oxide Layered Nanostructures.* Journal of the American Chemical Society, 1998. **120**(14): p. 3530-3531.

103. Huang, Q., C.M. Lilley, M. Bode, and R. Divan, *Surface and size effects on the electrical properties of Cu nanowires.* Journal of Applied Physics, 2008. **104**(2): p. 023709.

104. Lide, D.R., *CRC Handbook of Chemistry and Physics, 85th Edition*. 2004: Taylor & Francis.

105. Steinhögl, W., G. Schindler, G. Steinlesberger, and M. Engelhardt, *Size-dependent resistivity of metallic wires in the mesoscopic range.* Physical Review B, 2002. **66**(7).

106. Bid, A., A. Bora, and A. Raychaudhuri, *Temperature dependence of the resistance of metallic nanowires of diameter ⩾15nm: Applicability of Bloch-Grüneisen theorem.* Physical Review B, 2006. **74**(3).

107. Heltemes, E., *Far-Infrared Properties of Cuprous Oxide.* Physical Review, 1966. **141**(2): p. 803-805.

108. Kim, Y.-M. and J.-S. Lee, *Reproducible resistance switching characteristics of hafnium oxide-based nonvolatile memory devices.* Journal of Applied Physics, 2008. **104**(11): p. 114115.

109. Karabacak, T., J.S. DeLuca, P.-I. Wang, G.A. Ten Eyck, D. Ye, G.-C. Wang, and T.-M. Lu, *Low temperature melting of copper nanorod arrays.* Journal of Applied Physics, 2006. **99**(6): p. -.

110. Jiang, X., T. Herricks, and Y. Xia, *CuO Nanowires Can Be Synthesized by Heating Copper Substrates in Air.* Nano Letters, 2002. **2**(12): p. 1333-1338.

111. Septina, W., S. Ikeda, M.A. Khan, T. Hirai, T. Harada, M. Matsumura, and L.M. Peter, *Potentiostatic electrodeposition of cuprous oxide thin films for photovoltaic applications.* Electrochimica Acta, 2011. **56**(13): p. 4882-4888.

112. Pan, T.-M. and C.-H. Lu, *Forming-free resistive switching behavior in Nd_2O_3, Dy_2O_3, and Er_2O_3 films fabricated in full room temperature.* Applied Physics Letters, 2011. **99**(11): p. -.

113. Rashidi, A.M. and A. Amadeh, *Effect of Electroplating Parameters on Microstructure of Nanocrystalline Nickel Coatings.* Journal of Materials Science & Technology, 2010. **26**(1): p. 82-86.

114. McKenna, K. and A. Shluger, *The interaction of oxygen vacancies with grain boundaries in monoclinic HfO_2.* Applied Physics Letters, 2009. **95**(22): p. -.

115. McKenna, K., A. Shluger, V. Iglesias, M. Porti, M. Nafría, M. Lanza, and G. Bersuker, *Grain boundary mediated leakage current in polycrystalline HfO_2 films.* Microelectronic Engineering, 2011. **88**(7): p. 1272-1275.

116. Zhang, Y., H. Wu, Y. Bai, A. Chen, Z. Yu, J. Zhang, and H. Qian, *Study of conduction and switching mechanisms in $Al/AlO_x/WO_x/W$ resistive switching memory for multilevel applications.* Applied Physics Letters, 2013. **102**(23): p. 233502.

117. Prakash, A., D. Jana, and S. Maikap, *TaOx-based resistive switching memories: prospective and challenges.* Nanoscale Res Lett, 2013. **8**(1): p. 418.

118. Zhu, X.-J., J. Shang, and R.-W. Li, *Resistive switching effects in oxide sandwiched structures.* Frontiers of Materials Science, 2012. **6**(3): p. 183-206.

119. Sakamoto, T., K. Lister, N. Banno, T. Hasegawa, K. Terabe, and M. Aono, *Electronic transport in* Ta_2O_5 *resistive switch.* Applied Physics Letters, 2007. **91**(9): p. 092110.

120. Zheng, W., P.B. Griffin, J. McVittie, S. Wong, P.C. McIntyre, and Y. Nishi, *Resistive Switching Mechanism in* $Zn_xCd_{1-x}S$ *Nonvolatile Memory Devices.* Electron Device Letters, IEEE, 2007. **28**(1): p. 14-16.

121. Lee, C.B., B.S. Kang, M.J. Lee, S.E. Ahn, G. Stefanovich, W.X. Xianyu, K.H. Kim, J.H. Hur, H.X. Yin, Y. Park, I.K. Yoo, J.B. Park, and B.H. Park, *Electromigration effect of Ni electrodes on the resistive switching characteristics of NiO thin films.* Applied Physics Letters, 2007. **91**(8): p. 082104.

122. Herderick, E.D., K.M. Reddy, R.N. Sample, T.I. Draskovic, and N.P. Padture, *Bipolar resistive switching in individual Au–NiO–Au segmented nanowires.* Applied Physics Letters, 2009. **95**(20): p. 203505.

123. Lee, S., I. Hwang, S. Oh, S. Hong, Y. Kim, Y. Nam, K. Lee, C. Yoon, W. Kim, and B.H. Park, *Ultra-thin resistive switching oxide layers self-assembled by field-induced oxygen migration (FIOM) technique.* Sci Rep, 2014. **4**: p. 6871.

124. Yang, W.-Y. and S.-W. Rhee, *Effect of electrode material on the resistance switching of* Cu_2O *film.* Applied Physics Letters, 2007. **91**(23): p. 232907.

125. Gelderman, K., L. Lee, and S.W. Donne, *Flat-Band Potential of a Semiconductor: Using the Mott–Schottky Equation.* Journal of Chemical Education, 2007. **84**(4): p. 685.

126. Kirchartz, T., W. Gong, S.A. Hawks, T. Agostinelli, R.C.I. MacKenzie, Y. Yang, and J. Nelson, *Sensitivity of the Mott–Schottky Analysis in Organic Solar Cells.* The Journal of Physical Chemistry C, 2012. **116**(14): p. 7672-7680.

VITA

Sanaz Yazdanparast was born and raised in Tehran, Iran. After graduating from high school, Sanaz took the Iranian national exam to enter one of the top national universities in Iran. She was accepted in Shiraz University to continue her education in Materials Science and Engineering. In third year of her undergraduate program, Sanaz met her husband, Mohsen Asle Zaeem, who was a Master student in Shiraz University. In 2007, Sanaz received her Bachelor's degree in Materials Science and Engineering from Shiraz University. After graduation from Shiraz University, Sanaz received a research assistantship from the University of Malaysia, Kuala Lumpur to start her graduate study in Mechanical Engineering. In 2010, she received her Master's degree in Mechanical Engineering. While she was in Malaysia, she got married to Mohsen. In 2010, Sanaz moved to the United States of America, and in 2011, she started her Ph.D. study in Mississippi State University under supervision of Prof. Mark Horstemeyer. In August 2012, she moved to Rolla and joined Prof. Jay Switzer's research group at Missouri University of Science and Technology. Sanaz received her Ph.D. in Materials Science and Engineering in July 2015.